



**Beyond 2020 Heterogeneous Wireless Network with Millimeter-Wave Small-Cell Access and Backhauling**

Grant agreement n°619563

# Deliverable D1.3

## Dosimetric Aspects Related to the Human Body Exposure to Millimeter Waves

| | |
|---|---|
| **Date of Delivery:** | 31 December 2014 (Contractual) 18 December 2014 (Actual) |
| **Editor:** | UR1 |
| **Participant(s):** | UR1 |
| **Work package:** | WP1 – Heterogeneous wireless network with mmW small-cell access and backhauling |
| **Dissemination:** | Public (PU) |
| **Version:** | 1.0 |
| **Number of pages:** | 49 |

**Abstract:** In the context of fast development of millimetre-wave (mmW) technologies and concerns related to their possible impact on human health, this report provides a state-of-the art on the human body electromagnetic field exposure at mmW (target tissues, interaction at the air / skin interface, power absorption, propagation), mainly in V- and E-bands. Recent advances on mmW dosimetry are reviewed, and the key conclusions are summarized. A review of ICNIRP, IEEE and CENELEC guidelines for limiting exposure is also provided. The main considerations on which the guidelines are based (i.e. temperature, time, spatial averaging) are summarized and discussed. Numerical results on the interaction between the human skin and a plane wave in V- and E-bands are finally provided and discussed.

**Keywords:** mmW, electromagnetic field exposure, dosimetry, regulations, ICNIRP, IEEE, CENELEC, dielectric properties.

# Executive summary

This report is a deliverable of Work package 1 - Task 1.3 “Dosimetric aspects related to the human body exposure to millimeter waves”. It provides the state of the art on the human body electromagnetic field exposure at millimeter waves (mmW), as well as the summary of the current exposure limits and guidelines. The report includes the main considerations taken into account by regulations to establish the exposure levels (temperature, time, superficial and volume averaging, etc.).

Interactions between the human body and a plane wave in V- and E-bands are studied numerically. Data on reflection and transmission coefficients, as well as on the absorption in a homogenous skin model are quantified, and preliminary findings towards the analysis to be performed in Task 4.5 are summarized. In particular, it is shown that:

- The maximum power density occurs at the skin surface.
- The transmitted power attenuates exponentially in the skin and depends on the polarization and angle of incidence.
- Higher transmission values occur for parallel (TM) polarization than for perpendicular (TE) polarization.
- At normal incidence, about 62% of transmission is obtained in the V-band, while it increases up to about 68% in the E-band.

## Authors


| | | |
|---|---|---|
| **UR1** | Anda Guraliuc | anda.guraliuc@univ-rennes1.fr |
| **UR1** | Maxim Zhadobov | maxim.zhadobov@univ-rennes1.fr |
| **UR1** | Ronan Sauleau | ronan.sauleau@univ-rennes1.fr |

# Table of Contents

# List of Figures

# List of Tables

# List of Acronyms and Abbreviations

| Term | Description |
|---|---|
| **AH** | Aqueous Humor |
| **BRs** | Basic Restrictions |
| **CAD** | Computer Aided Design |
| **CEA** | Commissariat à l'Énergie Atomique et aux Énergies Alternatives (Atomic Energy and Alternative Energies Commission) |
| **CEN** | Comité Européen de Normalisation (European Committee for Standardization) |
| **CENELEC** | Comité Européen de Normalisation Électrotechnique (European Committee for Electrotechnical Standardization) |
| **CST MWS** | Computer Simulation Technology Microwave Studio® |
| **CW** | Continuous Waveform |
| **ELF** | Extremely Low Frequency |
| **EMF** | Electromagnetic Field |
| **FDTD** | Finite Difference Time Domain |
| **HPBW** | Half Power Beam Width |
| **ICNIRP** | International Commission on Non-Ionizing Radiation Protection |
| **IEEE** | Institute of Electrical and Electronics Engineers |
| **IPD** | Incident Power Density |
| **MPE** | Maximum Permissible Exposure |
| **mmW** | Millimeter Wave |
| **NIR** | Non-Ionizing Radiation |
| **NRPB** | National Radiological Protection Board |
| **PD** | Power Density |
| **RF** | Radio Frequency |
| **RL** | Reference Level |
| **SA** | Specific Energy Absorption |
| **SAR** | Specific Absorption Rate |
| **SC** | Stratum Corneum |
| **SGD** | Sweat Gland Ducts |
| **TE** | Transverse Electric |
| **TM** | Transverse Magnetic |
| **WiGig** | Wireless Gigabit Alliance |

## List of Definitions

| Term | Description |
|---|---|
| **Penetration depth** | • Is the depth at which the power density of radiation inside the material falls by $1/e^2$ (about 13%) of its original value at the surface. |
| **Basic restrictions (BRs)** | • Applied to exposure to time-varying electric, magnetic, and electromagnetic fields based directly on established health effects.<br>• The physical quantities used are the following:<br>- current density *J* [A/m$^2$]<br>- specific absorption rate *SAR* [W/kg]<br>- power density *PD* [W/m$^2$] |
| **Reference levels (RLs – terminology used by ICNIRP) or Maximum permissible exposure values (MPEs – terminology used by IEEE)** | • Provided for practical exposure assessment to determine whether the basic restrictions are likely to be exceeded.<br>• Some of the RLs (MPEs) are determined from the BRs using measurements or computations.<br>• The physical quantities are:<br>- electric field strength *E* [V/m]<br>- magnetic field strength *H* [A/m]<br>- magnetic flux density *B* [Wb/m$^2$]<br>- power density *PD* [W/m$^2$]<br>- current flowing through the limbs $I_L$ [A]<br>- contact current $I_C$ [A]<br>- specific energy absorption *SA* [J/kg] (is the time integral of specific absorption rate *SAR*; is considered for exposures to an EM pulse) |
| **Occupational public exposure limits** | • All exposures to EMF experienced by individuals in the course of performing their work.<br>• The person must be fully aware of exposure, must know how to control and limit the exposure and must have exposure training knowledge.<br>• Higher exposure limits apply. |
| **General public exposure limits** | • Apply to all consumer devices.<br>• There is no knowledge of exposure required.<br>• More restrictive exposure limits apply compared to occupational public restrictions. |
| **Specific Absorption Rate (*SAR*)** | • Represents the rate at which the energy is absorbed per unit mass of body tissue.<br>• Is expressed in watts per kilogram (W/kg).<br>• $\mathrm{SAR} = \frac{\sigma\left\|\vec{\mathrm{E}}\right\|^2}{\rho}$<br>σ – material conductivity [S/m]; $\vec{\mathrm{E}}$ – internal electric field (V/m); ρ - |

| | |
|---|---|
| | material density (kg/m$^3$) |
| **Power density (*PD*)** | • Represents the power per unit area normal to the direction of propagation.<br>• Is related to the electric and magnetic field as:<br>$\mathrm{PD}=\frac{\mathrm{P}}{\mathrm{S}}=\left\|\vec{\mathrm{e}}\times\vec{\mathrm{h}}\right\|$ in time domain<br>$\mathrm{PD}=\frac{1}{2}\mathrm{Re}\left\{\vec{\mathrm{E}}\times\vec{\mathrm{H}}^{*}\right\}$ in frequency domain<br>P – incident power (W), S – exposed surface area (m$^2$),<br>$\vec{\mathrm{E}}$ - electric field vector (V/m), $\vec{\mathrm{H}}$ - magnetic field vector (A/m).<br>This last formulation will be used throughout this document.<br>• Is expressed in watts per square meter (W/m$^2$).<br>• For uniform plane wave: $\mathrm{PD}=\frac{\left\|\mathrm{E}\right\|^2}{\eta}=\frac{\left\|\mathrm{E}\right\|^2}{377}$. |
| **ICNIRP** | • Represents the abbreviation for the International Commission on Non-Ionizing Radiation Protection. Is an independent organization, whose objective is to provide scientific advice and guidance on the health effects of non-ionizing radiation (NIR) to protect people from detrimental NIR exposure.<br>• Provides an overview of the physical characteristics, measurement and instrumentation, sources, and applications of NIR, a thorough review of the literature on biological effects, and an evaluation of the health risks of exposure to NIR. These health criteria have provided a scientific database for the subsequent development of exposure limits and codes of practice relating to NIR. |
| **IEEE Std.95** | • Is a document containing recommendations for safety levels with respect to human exposure to EMFs in the frequency range of 3 kHz to 300 GHz.<br>• Its purpose is to provide exposure limits to protect against established adverse effects to human health induced by exposure to RF electric, magnetic and electromagnetic fields over the frequency range of 3 kHz to 300 GHz. Its use is wholly voluntary. |
| **CENELEC** | • Represents the abbreviation for Comité Européen de Normalisation Électrotechnique (European Committee for Electrotechnical Standardization). Is an organization responsible for European standardization in the area of electrical engineering.<br>• Together with the European Committee for Standardization (CEN) and the European Telecommunications Standards Institute (ETSI), it forms the European system for technical standardization. |

# 1. Introduction

Over the last years, advances in millimeter-wave (mmW) technologies increased the interest of the research community in wireless applications at mmWs. Compared to the microwave spectrum, mmWs offer some advantages like compact, small antennas and devices (due to the small wavelength) that can support high data rates over distances as great as several km [1], [2]. Also, mmWs offer a high level of security for short range communications (due to high atmospheric attenuation), and reduced interference with other wireless services, devices and adjacent network cells.

Today, the cellular networks occupy the microwave spectrum, but since it is becoming very crowded, moving towards mmW spectrum would allow for larger channel bandwidths and data rates [3].

Future mmW integrated systems could have the attributes for new 5G mobile networks. Their use in cellular mobile networks will result in exposure of users at mmW frequencies, especially in the 57-66 GHz band if this frequency band is chosen for mobile access as proposed in MiWaveS vision. However, mmW systems must be compliant with standards (e.g. IEEE 802.11, IEEE 802.15, IEC 62209-1) based on the ICNIRP, IEEE and CENELEC exposure limits and recommendations. In V- and E-bands, according to ICNIRP recommendations, the relevant dosimetric quantity to be considered is the incident power density (IPD). The recommended limits are 1 $mW/cm^2$ for general public, while for the occupational exposure the limit is 5 $mW/cm^2$. Both values are averaged over 20 $cm^2$ of exposed area [4], [5]. Also, for local exposure, the spatial maximum PD, averaged over 1 $cm^2$, should not exceed 20 times the values listed above. Similar restrictions are adopted by the CENELEC [6-9] / IEEE [10] regulations with some differences discussed in Section 3. It should be noted that previous recommended limits are based on investigations related to possible induced biological effects due to EM exposure. In particular, studies on the eye at microwaves, where cataract may appear [11], were considered to establish the limits at mmW. The recommended levels at mmW are applied to both target organs, i.e. eye and skin. Current recommendations for mmW do not provide limit values for near-field exposure, but only for far-field exposures. Compared to the microwave spectrum, the Specific Absorption Rate (SAR) is not used as a dosimetric quantity at mmW. However, it can be used as an intermediate parameter to retrieve the incident and in-tissue PD.

The main purpose of this report is to provide an overview of the scientific literature, guidelines and standards related to the mmW / human body interactions. It also underlines the most appropriate dosimetric quantities and the exposure limits to be considered. Preliminary numerical results are also presented in the report regarding the propagation of plane waves in V- and E-bands into the human skin, since the latter is the most exposed part of the body at these frequencies.

The report is organized as follows. In Section 2, the interaction mechanism of mmW with biological tissues is described. mmW dosimetry aspects are also reviewed. Insights into the reflection and transmission at the air / skin interface, as well as influence of clothing are provided in the same section. mmW exposure limits defined by ICNIRP, IEEE and CENELEC are summarized in Section 3. In Section 4, rationales and considerations behind these limits and recommendations are discussed. Section 5 provides results of a numerical study on the propagation of plane waves in V- and E-bands into the human skin. Data on reflection and transmission coefficients, as well as absorption in the skin are quantified. Section 6 provides some insights into the numerical modeling at mmWs.

Conclusions are drawn in Section 7. Section 8 draws the steps to be followed in Task 4.5 "Exposure assessment and evaluation of antenna / human body interactions".

Table 1.1 summarizes the key points related to mmW dosimetry and exposure assessment.

**Table 1.1**: Key points.

**Interaction of mmW with the human body (Sections 2.1-2.5)**

- At 60 GHz under normal incidence, **around 40% of the incident power is reflected by the skin**. Transmission is strongly correlated to the wave polarization and angle of incidence.
- **The penetration depth in biological tissues** is very shallow at mmW (e.g. at 60 GHz the depth penetration is around 0.5 mm), and power is absorbed by superficial layers of the body.
- As a consequence, **the main target tissues** for mmW are skin and cornea.
- Shallow penetration depth of mmWs in the skin induce **SAR levels significantly higher than those at microwaves** for identical IPD values (e.g. 100 W/kg for an IPD of 1 mW/cm$^2$ at 60 GHz).

**Heating due to the exposure to mmW (Section 2.7)**

- Average and high-power mmW exposures (above 10 mW/cm$^2$, and average over 20 cm$^2$) may result in a significant **temperature increase** (above 1°C), which might induce cataracts, ocular lesions or inflammation, corneal opacity, epithelial injury, miosis, changes in vascular permeability, skin burns, dermis tissue damage. *The expected power levels corresponding to wireless communications are sufficiently low, so that the skin and eye heating does not exceed several tenths of °C*.

**Influence of clothing (Sections 2.8-2.9)**

- The presence of clothing in direct contact with human skin may induce an increase of power transmission coefficient. However, the presence of an air gap between skin and clothing decreases the power transmitted to the skin.
- Path gain variations related to regular textile presence (typically 0–5 dB along the body propagation) are lower than the changes of the path gain on a real human body occurring due to the different postures, movements, and positioning of antennas (typically above 10 dB).

**Guidelines for exposure limits and considerations (Section 3 & Section 4)**

- At mmW, absorption is very superficial. As a consequence the safety guidelines are set in terms of the maximum accepted **incident power density** (IPD).

**Basic restrictions (BRs)**

| Organization | Frequency (GHz) | Public exposure | Power density (mW/cm$^2$) | Averaging | |
|---|---|---|---|---|---|
| | | | | Surface (cm$^2$) | Time (min) |
| **ICNIRP** | 10-300 | Occupational | 5 | 20 | $68/f^{1.05}$ |
| | | | 100 | 1 | |
| | | General | 1 | 20 | |
| | | | 20 | 1 | |
| **IEEE** | 30-300 | Occupational | 10 | 100 | $25.24/f^{0.476}$ |
| | | | 100 | 1 | |
| | 30-100 | General | 1 | 100 | |
| | | | 100 | 1 | |
| **CENELEC** | 2-300 | Occupational | 5 | 20 | $68/f^{1.05}$ |
| | | | 100 | 1 | |

| | | | | | | | |
|---|---|---|---|---|---|---|---|
| | | | General | 1 | 20 | | |
| | | | | 20 | 1 | | |
| | $f$ – frequency in GHz | | | | | | |

**Comparison of V- and E-bands (Section 5)**

- For a normally incident plane wave at the air / skin interface:

| Frequency (GHz) | Penetration depth $\delta$ (mm) | Power transmission coefficient % | Max power density in the skin $PD$ (mW/cm$^2$) | |
|---|---|---|---|---|
| | | | 1 mW/cm$^2$ | 5 mW/cm$^2$ |
| **60** | 0.48 | 63 | 0.62 | 3.12 |
| **74** | 0.42 | 65 | 0.65 | 3.26 |
| **84** | 0.39 | 68 | 0.68 | 3.38 |

# 2. Fundamentals on the interaction of mmW with the human body

The interaction of the EMFs with the human body depends on frequency, electromagnetic field strength and power, type of exposure (CW or pulsed), and duration. In order to evaluate the human exposure to EMF, quantities like *SAR*, *induced electric field* and *current density* have been used for dosimetry at low frequencies and at microwaves. It has been shown that, in addition to the exposure parameters, these quantities depend on the tissues type. Usually, a region of specific tissue mass (i.e. 1 g or 10 g) is used for SAR averaging and correlation with induced biological effects. For instance, 10 g of tissue correspond to a cube with edge dimension 2.15 cm (which volume is about 10 $cm^3$) [10], where induced effects like cataract have been noticed [11].

At mmW, the primary target organs / biological tissues are eyes and skin. Above 30 GHz, the absorbed power is superficial (penetration depth is 1 mm or less), mainly due to the relaxation of free water molecules occurring at these frequencies. For instance, at 60 GHz, penetration depth is around 0.5 mm, so the penetration is limited to the superficial layers of the human skin and cornea. As a consequence, incident power density (IPD) has been used as a dosimetric quantity at mmW. The shallow penetration at mmW results in SAR levels significantly higher compared to those at microwaves for the same IPD, possibly leading to a significant superficial heating.

## 2.1 Interaction with eyes

This section reviews some of the main research studies performed on the EMF exposure of the eyes, both at microwaves and mmWs. This review is necessary since some of the safety limits recommendations for local exposures are based on thermal effects in the eyes which have been examined extensively in the microwave region.

High-power RF energy can cause some ocular effects in the eye (which diagram is shown in Figure 2-1), in particular cataracts [11], but also effects on retina, cornea and other ocular systems may occur.

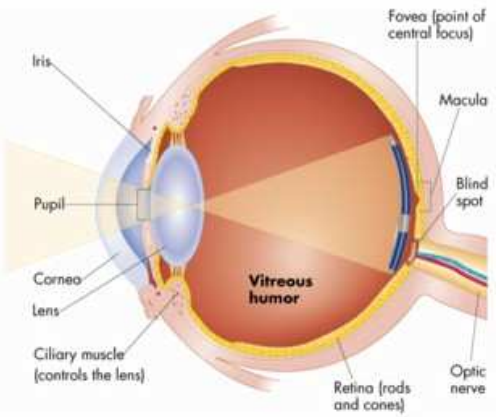


**Figure 2-1**: Schematic diagram of human eye.

During the years, experiments on animal eyes have been performed considering localized, very high RF fields. A correlation between the average SAR in the eye and the temperature elevation was established. For example, exposures at 2.45 GHz for more than 30 min at IPD of 150 $mW/cm^2$ can cause high SAR levels (138 W/kg) and temperatures (> 41°C) in or near the lens causing cataracts in rabbit eyes [12]. Many experiments, performed at 2.45 GHz showed that an IPD larger than 100 $mW/cm^2$ for 30 min can induce lens opacity [13]. However, opacity in the eyes of monkeys has

not been observed after repeated acute localized exposure of up to 500 mW/cm$^2$, well above threshold levels for rabbits. Monkeys were exposed to 2.45 GHz CW for up to 12 h over four months period at SAR in the head of up to 40 W/kg. After 1-4 years eye continuous examinations, no effects on the lens have been revealed. The lower susceptibility of monkeys to cataract is due to the structural differences in the two species eyes and skull, resulting in low SAR and temperature increase [14].

Temperature elevations have also been numerically investigated [15]-[18]. In [16] a numerical human head model is considered for SAR and temperature distribution in the eye. It is shown that at 2.45 GHz, a SAR of 2 W/kg (general public) or 10 W/kg (occupational public) averaged over 10 g of tissue, induced a temperature increase of 0.3°C or 1.5°C in the lens [16]. In [18] a numerical investigation has been performed to evaluate the SAR and temperature distributions for possible systems operating between 6 and 30 GHz. In [18], a numerical study performed on a human head model revealed that, for an IPD of 1 mW/cm$^2$ applied to the eye, the maximum temperature increase is about 0.6°C in the lens at the frequencies of 18 and 30 GHz. An IPD of 10 mW/cm$^2$ induces a maximum temperature increase of 0.3°C in the lens at 6 and 18 GHz, while 0.5°C temperature increase in the cornea is found at 18 GHz. While at 2.45 GHz the radiation penetrates sufficiently deep into the eye (the eye's part most at risk being the inner region, i.e. lens, vitreous humor), moving towards higher frequencies where the radiation penetration depth is smaller, a greater power deposition takes places in the cornea. Normal temperature in the cornea has been both numerically and experimentally determined to be around 32-33°C. The noted temperature increment values are much less than the threshold value of 3-4°C to induce cataract. In [19], it was also shown that, for plane wave exposures at 6 GHz, for an IPD of 5 mW/cm$^2$, a maximum temperature elevation of 0.3°C appears near the eye surface.

The ICNIRP [5] guidelines considered the National Radiological Protection Board (NRPB) document [17]. The latter, based on Hirata's studies [19]-[20], concluded that in the frequency range 0.6-6 GHz, at 1 W/kg averaged over the eye may lead to a steady-state temperature increase of 0.4°C. At 10 W/kg the temperature increase in the eye would be 4°C if only the eye without the head is considered. To be noted that, normal temperature in the eye is about 37.8°C.

Most of the studies performed at frequencies below 30 GHz showed that an IPD of 100 mW/cm$^2$ lasting at least 30 min can induce cataract. Temperature threshold for cataract has been established at around 41°C, which corresponds to a temperature increase of about 3-4°C in the eye.

Some recent studies have been performed at mmW [21]-[27]. In [24], rabbit eyes were exposed to a source represented by a horn antenna at 60 GHz capable of supplying an IPD of 10 mW/cm$^2$. Post-exposure diagnostic examination of rabbit eyes after acute (8 h exposure) and repeated (five separate 4 h exposure) **60 GHz CW exposure at 10 mW/cm$^2$ (averaged over 20 cm$^2$) did not reveal any ocular changes.** More recently, in [23], similar conclusions have been outlined for rabbit eyes after *in vivo* exposures to 200, 100, 75, 50, 10 mW/cm$^2$ at 76 GHz CW for 6 min with a lens antenna. Corneal opacity, epithelial injury, miosis, and ocular inflammation were present up to 2-3 days after exposure at 200 mW/cm$^2$; no ocular changes other than reversible corneal **epithelial injury were seen following exposures at 100 and 75 mW/cm$^2$; no ocular changes after exposure at doses of 50 or 10 mW/cm$^2$.**

In [25], a detailed dosimetry of the human eye exposed to 77 GHz mmW was presented. A maximum SAR of 45.1 W/kg (averaged over 10 g) was found in the eye for an IPD of 1 mW/cm$^2$. Using

an infrared imaging system (used to record remotely the surface temperature with a high sensitivity (<50 mK)), the exposure from a horn antenna induces a maximum increase of 0.7°C for a PD of 10 mW/cm$^2$ and less than 0.1°C for 1 mW/cm$^2$ for porcine eye (*in vitro*).

Numerical modeling of heat in the human / rabbit eye under mmW exposure was analyzed in [26], [27]. The model takes into account the fluid dynamics of the aqueous humor (AH) and predicts a frequency and IPD dependency to reverse its flow. In the rabbit eye, a temperature difference of 0.02°C between the front and back surface of the anterior chamber was sufficient to induce circulation of the AH. At 60 GHz, the study revealed that for IPD between 10-50 mW/cm$^2$ the direction of the AH flow is counter clock wise, with a temperature in the cornea from 34°C to 36.4°C. The flow direction changes for PD from 60-160 mW/cm$^2$, and temperatures are between 36.8°C - 40.9°C. Apparently, the temperature increases linearly with the IPD of about 0.4°C / 10 mW·cm$^2$. To be noted that, normal temperature in the cornea is about 32-33°C. The predicted temperature rise for the human eye is however lower than the temperature rise computed for the rabbit eye.

Table 2.1 summarizes the related studies to the eye effects to EMF exposure.

**Table 2.1**: Related studies to the eye effects due to EMF exposure.

| **Microwaves** | | | | | | | | |
|---|---|---|---|---|---|---|---|---|
| Frequency [GHz] | Species | Power density [mW/cm$^2$] | SAR [W/kg] | Exposure | Study | Temperature gradient [°C] | Effect | Ref. |
| 2.45 | Rabbit eye | 150<br><br><br>295 | 138<br><br><br>- | 1 day exposure for 100 min<br>1 day exposure for 30 min | Experimental | 6 | cataract | 12 |
| 2.45 | Monkey eye | 150 | - | 1 day exposure for 30 min | Experimental | | No effect | 14 |
| 2.45 | Human eye | | 2<br>10 | - | Numerical | 0.3 in lens<br>1.5 in cornea | - | 16 |
| 6 | Human eye | 10 | 1.68 | - | Numerical | 0.3 in lens | - | 18 |
| 18 | Human eye | 10 | 13 | - | Numerical | 0.5 in cornea | - | 18 |
| **Millimeter waves** | | | | | | | | |
| 60 | Rabbit eye | 10 | - | 8 hours | Experimental | | No effect | 24 |
| 60 | Rabbit and Human eye | 60-160 | - | - | Numerical | 0.4°C / 10 mW/cm$^2$ | Change of the aqueous humor fluid dynamics direction | 26,27 |
| 76 | Rabbit eye | 200<br>100<br>75<br><br>50<br>10 | - | 6 min | Experimental | 9-10<br>5<br>4<br><br>0.5 | Corneal opacity<br>Reversible corneal, epithelial injury<br>No effect<br>No effect | 23 |
| 77 | Human & Porcine eye | 1<br>10 | 45.1 | - | Numerical & Experimental | 0.1<br>0.7 | No effect | 25 |

- **Recent *in vivo* studies performed at mmW revealed that exposure at 100 mW/cm$^2$ can induce reversible corneal epithelial injury, while exposure at 50 mW/cm$^2$ and 10 mW/cm$^2$ did not induce any ocular tissue damage. The averaging area is 20 cm$^2$. It should be noticed that for IPD values 10-50 times higher than the recommended levels (i.e. 1 mW/cm$^2$ for general public and 5 mW/cm$^2$ for occupational public) no ocular effects were observed.**
- **Temperature increase of about 0.1°C or 0.7°C are expected for exposures at 77 GHz and for IPD of 1 mW/cm$^2$ and 10 mW/cm$^2$, respectively.**
- **Majority of the current studies showed that as long as the exposure is in the recommended limits (i.e. for local exposure scenario, IPD averaged over 1 cm$^2$: 20 mW/cm$^2$ for general public and 100 mW/cm$^2$ for occupational public), the temperature increase does not exceed the temperature threshold (i.e. 41°C) where cataract in the eye may occur.**

## 2.2 Interaction with human skin

About 95% of the human body is covered by skin and therefore this is the main target for mmW exposure due to the shallow penetration limited to several tenths of a millimeter. The skin (schematic diagram shown in Figure 2-2) is composed in average of 65.3% free water, 24.6% proteins and 9.4% lipids, and consists of three different layers: epidermis (thickness 0.05 mm on the eyelids up to 1.5 mm on the palms and soles), dermis (thickness 0.3 mm on the eyelid up to 3 mm on the back) and subcutaneous tissue (thickness 1.1 mm to 5.6 mm) [28].

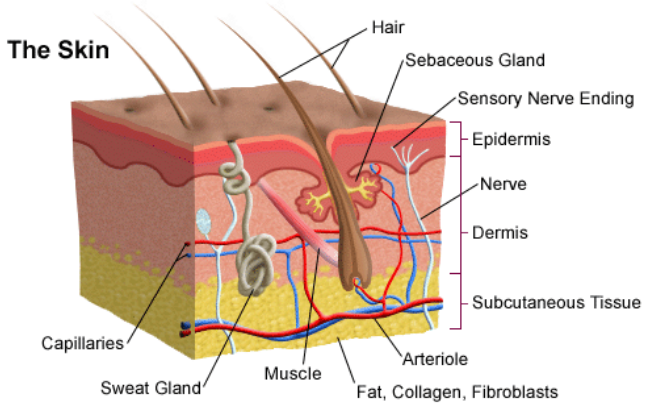


**Figure 2-2**: Schematic diagram of human skin.

In [22], theoretical parametric analyses of temperature elevation due to mmW exposure have been performed in a single-layer model of the skin and a three-layer model (skin/ fat/muscle). CW and normal incidence were assumed. An approximated analytical solution of the bioheat equation was used to evaluate the temperature elevation in the frequency range 30-300 GHz for an IPD of 5 mW/cm$^2$. It was stated that the temperature increase on the body surface decreases monotonically with thermal parameters (terms associated with the blood flow, thermal conductivity and heat transfer coefficient). At 60 GHz the maximum temperature increase at the skin surface (for the skin-layer model) was found to be 0.7°C. In the three-layer model, the maximum temperature increase was 2 times higher than in the single layer model (i.e. 1.4°C at the skin surface). It was also shown

that the heat transfer coefficient is the dominant parameter in temperature change in the three-layer model. Theoretical analysis on the steady-state temperature elevation using bioheat equation shown that this depends on many parameters: thermal conductivity, blood flow, thermal and tissues thickness parameters etc. In a 3-layer model (skin/fat/muscle) a temperature elevation for a maximum condition to reach an increase of 2-3 times higher than in a single layer model might occur. This finding can be an informative explanation for the variability of warmth sensation. One dimensional model simplification is reasonable since the heat diffusion length in biological tissues is at most a few mm. Moreover, experimentally has been shown that temperature elevations appear at the skin surface.

The presence of cutaneous blood vessels affects mmW-induced heating of the skin. The orientation of the exposed vessels with respect to the E-field of the incident mmW energy has a significant effect. The greatest temperature rise for an exposure to an IPD of 10mW/cm$^2$ averaged over 20 cm$^2$ (i.e. 4.7°C) occurs with vessels oriented parallel to the direction of the E-field [29], [30]. Also, the blood flow greatly affects the temperature rise resulting from mmW exposure. In [29], an "effective" thermal conductivity has been added to the bioheat equation to quantify mmW heating of the skin at high blood flow rates. The presence of a fat layer resulted in the appearance of a significant temperature gradient between the dermis and muscle layer which increased with the fat layer thickness (e.g. at 42 GHz an IPD of 20 mW/cm$^2$ may generate an increase of 2.5°C for a 2 mm fat thick layer or 3.5° for 8 mm fat thick layer, an increase which is however below the threshold 41°C) [31], [32].

At 60 GHz, a plane wave normally incident on the surface of a single layer or multilayer skin model was considered in [29]. It was shown that, for a 2 mm-thick skin, it is possible to calculate the PD, penetration depth and SAR. The thin (10μm to 40μm thickness) stratum corneum (SC) has little influence on the interaction of mmW with skin. On the contrary, the thick SC in the palm played the role of a matching layer and significantly increased the power deposition. The epidermis and dermis contain a large amount of free water, and as a consequence mmW energy is highly attenuated. The greatest SAR was noticed at the superficial layer of the skin (e.g. about 150 W/kg at 0.1 mm depth for IPD of 10 mW/cm$^2$).

The SAR distribution and thermal response in the human skin in W-band was also addressed in [25] for a plane wave exposure. An analytical method was used to investigate SAR inside a layered model of the human skin from 3 to 100 GHz. For an IPD of 1 mW/cm$^2$, the maximum SAR was found to be 27.2 W/kg in skin. The temperature changes of the superficial tissue caused by a horn antenna were measured using an infrared imaging system. The study showed that, at 77 GHz for an IPD of 10 mW/cm$^2$, the temperature increase is about 0.7°C, and for an IPD of 1 mW/cm$^2$ the increase is less than 0.1°C in human skin (*in vivo*). Moreover, in [33], it was shown that exposure at 60 GHz produces a skin temperature increase of about 0.1°C for an IPD of 1 mW/cm$^2$ and 0.5°C for IPD of 5 mW/cm$^2$ (the exposure limit for the occupational environment for 20 cm$^2$).

In [34], a numerical modeling of the mmW propagation and absorption in a high resolution skin model was investigated. The purpose was to investigate the potential effect of sweat gland ducts (SGD) on SAR and temperature distributions during mmW exposure. This study presented an improvement in the higher spatial resolution numerical modeling of the skin, showing that microstructures can play a significant role in the mmW absorption and induced temperature. The results showed that SGD could act as a high absorption site for mmW radiation, in agreement with

previous studies [22]. It was noticed that, when SGD is included in the skin model, at 94 GHz, a maximum SAR of 288000 W/kg is obtained in the SGD. Assuming a linear relationship between SAR and temperature gradient, the maximum temperature increase of about 32°C within the center SGD would be expected. However, in the considered model only an increase of 7°C was calculated. To be noted that, initial condition for the temperature was 32°C [35]. The discrepancy in the increased temperature is due to a very high SAR in an extremely local area (<0.01 $mm^3$) at the tip of the SGD, which included only a few voxels. In thermal simulation, these few voxels would represent a very small heating source inducing a rapid heat dissipation, and as a consequence a lower temperature increase. The maximum temperature increase calculated in [34] was in agreement with the temperature measured in the skin of healthy volunteers [36]. In [36], the skin temperature increase of roughly 10°C was measured after 3s exposure to 18 $kW/m^2$ at 94 GHz. In [34], the temperature increase of about 4.5°C was calculated for 3s exposure at 9.3 $kW/m^2$ of 94 GHz. The steady-state temperature increase (7°C) was reached after about 20s of continuous exposure to 94 GHz irradiation.

- Majority of the studies showed that **mmW radiation is mainly absorbed in the epidermis and upper dermis.**
- Shallow penetration of mmWs in the skin results in **SAR levels significantly higher than those at microwaves for identical IPD values** (e.g. 150 W/kg (60 GHz) for an IPD of 10 $mW/cm^2$ compared to 8-10 W/kg (2.45 GHz) averaged over 10 g of tissue).
- For the exposure limits, **the following typical skin temperature increases have been demonstrated:**
  - General public 1 $mW/cm^2$: an increment of 0.1°C.
  - Occupational public 5 $mW/cm^2$: an increment of 0.5°C.
  - 10 $mW/cm^2$ (level usually used in RF therapy): an increment of 0.7° C to 1°C.
    **N.B. averaging surface area is 20 $cm^2$.**
- Temperature distribution at mmW depends on the geometrical and thermal properties of the multilayer skin model. In particular, heating is related to the blood flow, sweet gland ducts, fat and muscle layer. The environmental temperature and physiological conditions impact the temperature distribution, and corresponding steady-state increment may vary by a factor of 3. However, **for IPD recommended by the ICNIRP/IEEE/CENELEC, the temperature increases are much lower than environmental thermal fluctuations.**

**In the following, the attention will be mainly focused on skin as this is the most exposed organ in the considered MiWaveS exposure scenarios. Also, the highest exposure levels are expected to occur in the skin. If needed, eyes will be included in the numerical modeling of Task 4.5.**

## 2.3 Dielectric properties of human skin

The knowledge of the dielectric properties of human skin is essential to determine the reflection, transmission and absorption of mmW in the human body, as well as for the electromagnetic modeling and dosimetry. Available data for the skin permittivity at mmW, in particular above 50 GHz, are very limited due to technical difficulties in measuring this parameter. The dispersive behavior of the dielectric properties of biological tissues is related to the rotational dispersion of free water molecules [37]. The results on skin permittivity presented so far in the literature strongly depend on the measurement technique, type of study (*in vivo* or *in vitro*), experimental conditions (e.g. skin temperature, location on the body, thickness of different skin layers etc.).

In [38], *Gabriel et al.* reported the complex permittivity of the human skin up to 110 GHz, based on an extrapolation of measured data performed up to 20 GHz on *in vivo* human skin. Two skin models have been identified: *wet skin* and *dry skin*. For the *wet skin* data, a gel has been used to moisture the skin. *Dry skin* model corresponded to human skin under normal environmental and physiological conditions (T ~ 32.5°C). In [39], an extrapolation of the measured data on rabbit skin at 23 GHz using a Debye model is performed at 60 GHz. *In vitro* studies on human skin samples have been performed in [40], and the dielectric properties were obtained using a free space quasi-optical technique in the 60-100 GHz frequency range.

*In vivo* measurements on the epidermis of the human palm and wrist were performed in [41] using a coaxial probe up to 110 GHz.

Reflection measurements with an open-ended waveguide were carried out in [42] by *Alekseev et al.* considering the forearm and palm skin. Homogeneous and multilayer models were proposed to fit the experimental data. More recently, in [43], a new method to determine the dielectric properties of human skin based on heating kinetics has been introduced. Forearm skin is exposed at 60.4 GHz using an open-ended waveguide and CW signal. Temperature distribution is recorded using an infrared camera. By fitting the analytical solution of the bio-heat transfer equation to the experimental heating kinetics, the values of power density and penetration depth can be defined. The latter is used to retrieve the complex permittivity of the skin described by Debye equation. This method has been also validated through measurements using an open-ended slim coaxial probe designed to operate up to 67 GHz.

Table 2.2 summarizes the skin dielectric complex permittivity at 60 GHz. Generally, Gabriel's model is the well-established model and is widely used as a reference.

Dry skin permittivity according to Gabriel's data is shown in Figure 2-3 over a broadband frequency range from 50 to 90 GHz. The complex dielectric permittivity is given by the Debye equation:

$$\varepsilon^* = \varepsilon_\infty + \frac{\Delta\varepsilon}{1 + j\omega\tau} + \frac{\sigma}{j\omega\varepsilon_0}, \tag{1}$$

where $\omega = 2\pi f$, $f$ (Hz) is the frequency, $\Delta\varepsilon = \varepsilon_S - \varepsilon_\infty$ is the magnitude of the dispersion of the free water fraction of skin, $\varepsilon_S$ is the permittivity at $\omega\tau << 1$, $\varepsilon_\infty$ is the optical permittivity and is equal to $2.5+2.7w_t$ with $w_t$ being the weight fraction of the total water content of the material to be characterized, $\tau$ is the relaxation time, $\sigma$(S/m) is the ionic conductivity. Debye parameters in the frequency range 50-90 GHz are: $\varepsilon_\infty = 4$, $\varepsilon_S = 32$, $\tau = 6.9$ ps, $\sigma = 0.2$ S/m.

**Table 2.2**: Skin dielectric properties at 60 GHz.

| $\varepsilon^*$ | T [°C] | Method | Study | Reference |
|---|---|---|---|---|
| 7.98 - j·10.90 | 32.5 ± 0.5 | Extrapolation | *In vivo* (*dry skin*) | Gabriel [38] |
| 10.22 - j·11.84 | 37 | Extrapolation | *In vitro* (*wet skin*) | Gabriel [38] |
| 8.89 - j·13.15 | 37 | Extrapolation | *In vitro* | Gandhi [39] |
| 8.05 - j·4.13 | 24-26 | Measurement | *In vivo* | Hwang [41] |
| 9.90 - j·9.00 | 23 | Measurement | *In vitro* | Alabaster [40] |
| 13.2 - j·10.30 | 37 | Extrapolation | *In vitro* | Alabaster [40] |
| 8.12 - j·11.14 | 20-22 | Measurement | *In vivo* | Alekseev [42] |
| 8.02 - j·10.05 | 32-33 | Measurement | *In vivo* | Chahat [43] |

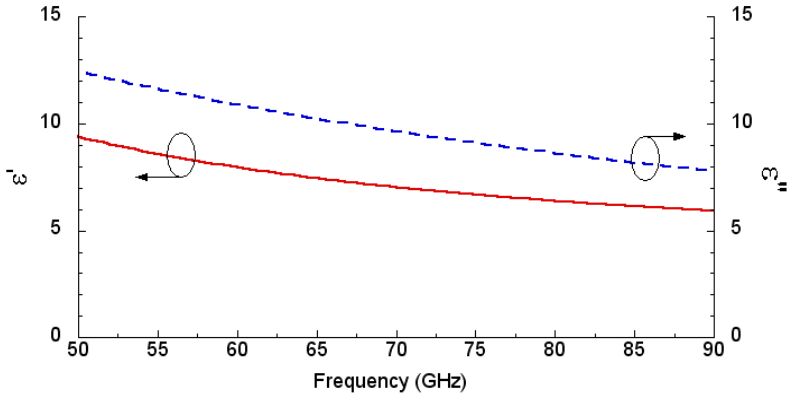


**Figure 2-3**: Complex permittivity of the dry skin in 50-90 GHz range [38].

- **Wet and dry skin dielectric permittivity data are available in V- and E-bands.**
- **The broadband behavior can be described by the Debye's model.**
- **At 60 GHz the skin complex permittivity is $\varepsilon^* = 7.98 - j \cdot 10.90$ (Gabriel's data).**

## 2.4 Skin phantom

Generally, in order to evaluate the exposure of the human body to EMF, phantoms simulating the properties of the human tissues are used. Indeed, different phantoms have been proposed and classified [44-54]. Liquid or gel phantoms have been widely used for frequencies up to 10 GHz. They are easy to prepare and allow for an easy scan of the E-field inside the phantoms. One of the disadvantages is the poor stability of the dielectric properties due to water evaporation. Although solid dry phantoms with fine stability have also been developed up to 6 GHz, they require complex and skilled procedures and lead to high cost [49], [50].

At mmW, liquid phantoms are of limited interest because of the container and very shallow penetration of the field into the tissue (i.e. $\delta_{60GHz} \approx 0.5$ mm).

It was demonstrated that at higher frequencies, the interaction with the human body is limited to the skin [29-31], [33]. As a consequence, a semi-solid skin-equivalent phantom has been recently proposed in [55] for dosimetric studies at mmW. Its composition (based on deionized water, agar,

polyethylene powder, TX-151, and sodium azide) has been optimized to coincide with measured values of the human skin permittivity in V-band. Its dielectric properties have been measured using an open-ended slim coaxial probe designed for permittivity measurements of liquids and semisolids up to 67 GHz. The phantom permittivity measured at 60 GHz was found $\varepsilon^* = 7.4 - j\cdot 11.4$, with an error of 7.3% for the real part and 4.6% for the imaginary part compared with the Gabriel's target data [38]. These deviations have been proven to be acceptable for antenna measurement, channel propagation and dosimetric studies, since they lead to small variations of the power reflection coefficient, penetration depth, and SAR [55-57].

Furthermore, a solid phantom emulating the same reflection coefficient as the one of skin was recently reported for the 58-63 GHz range [58]. While it cannot be directly used for the dosimetry, it can be used to evaluate the distortion of the terminal performances due to the presence of the human body.

**A semi-solid phantom emulating dry skin dielectric properties is available at 60 GHz for experimental dosimetric studies. Solid phantom covering 58-63 GHz range can be used to evaluate the distortion of the terminal performances due to the presence of the human body.**

## 2.5 Reflection and transmission at the air / skin interface

As previously mentioned, the skin dielectric properties have a significant impact on the reflection and transmission coefficients at the air / skin interface. In [33], the reflected and transmitted coefficients are reviewed for a 60-GHz plane wave illuminating a semi-infinite flat model with dielectric properties of the skin.

Two cases are considered as shown in Figure 2-4:

a) Parallel polarization (TM mode), where the $\vec{E}$ field is parallel to the plane of incidence,
b) Perpendicular polarization (TE mode), where the $\vec{E}$ field is perpendicular to the plane of incidence.

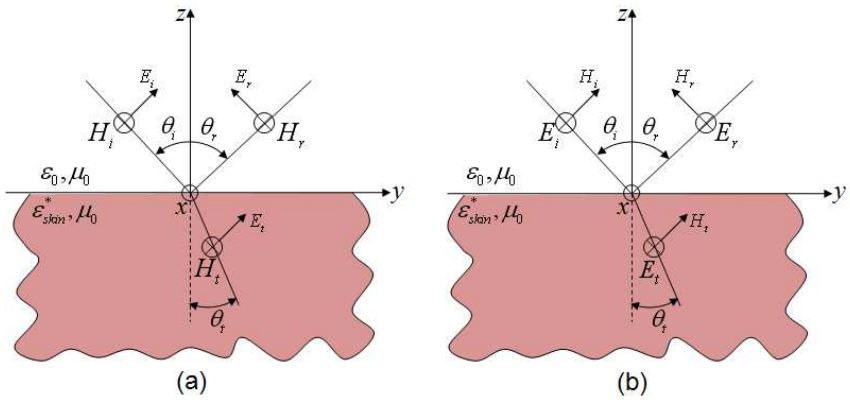


**Figure 2-4**: Polarization: (a) parallel (TM); (b) perpendicular (TE).

Figure 2-5 represents the power reflection and transmission coefficients calculated analytically at 60 GHz at the air / skin interface. A homogeneous skin model with dielectric properties known from the literature is considered. In particular, the following skin permittivities are chosen: $\varepsilon^* = 7.98$ -

j·10.90 [38], ε* = 8.89 - j·13.15 [39] and ε* = 8.05 - j·4.13 [41]. It is shown that the reflected power depends on the polarization and angle of incidence. It is interesting to notice that, for normal incidence, the incident power reflected from the skin is about 38% for the Gabriel model, 40% for Gandhi's model, and 28% for Hwang's model. The power absorbed by the skin is 62% (Gabriel), 60% (Gandhi) and 72% (Hwang), respectively.

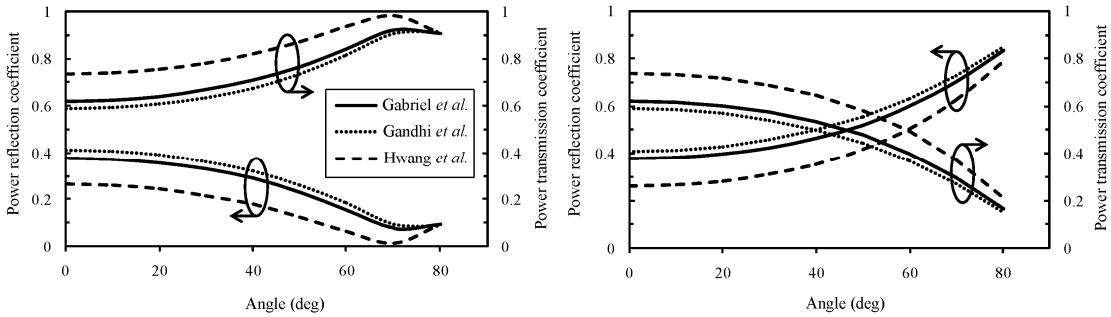


**Figure 2-5**: Power reflection and transmission coefficients at the air / skin interface at 60 GHz for: (a) parallel polarization and (b) perpendicular polarization [33].

## 2.6 Absorption in skin

The transmitted power decreases exponentially in the skin as a function of depth. The PD at a depth *z* within skin is given by:

$$PD(z) = PD_0 \cdot e^{-2z/\delta} = IPD \cdot \left(1 - |\Gamma|^2\right) \cdot e^{-2z/\delta}, \quad (2)$$

where $PD_0$ is the power density at the surface, $|\Gamma|^2$ is the power reflection coefficient, and $\delta$ is the penetration depth.

A plane wave illuminating a homogeneous skin model at 60 GHz is considered in [33]. The attenuation of PD and SAR for an incident power of 1 mW/cm$^2$ is shown in Figure 2-6. For the Gabriel's and Gandhi's models, 40% of the incident power arrives into dermis and 0.1% into the fat layer, while, for the Hwang's model, 60% reaches the dermis and 10% the fat layer. These results confirm that only epidermis and dermis have to be used for EM dosimetry. Similar conclusions were reported in [59], where a detailed analysis regarding the main characteristics (reflection, power density, penetration depth, and SAR) of mmW skin dosimetry was conducted for an homogeneous model (epidermis-dermis) and for two multilayer models (SC-epidermis-dermis and SC-epidermis-dermis-fat, respectively). In particular, the forearm and palm data were used to model the skin with thin and thick stratum corneum (SC). It was shown that epidermis and dermis highly attenuated mmW. This was expected since these tissues have a large amount of free water. It was also shown that the fat layer has an insignificant impact on the PD and SAR profiles. This study concluded that mmWs penetrate into the human skin deep enough (penetration depth ~ 0.5 mm at 60 GHz) to affect most skin structures located in the epidermis and dermis [59].

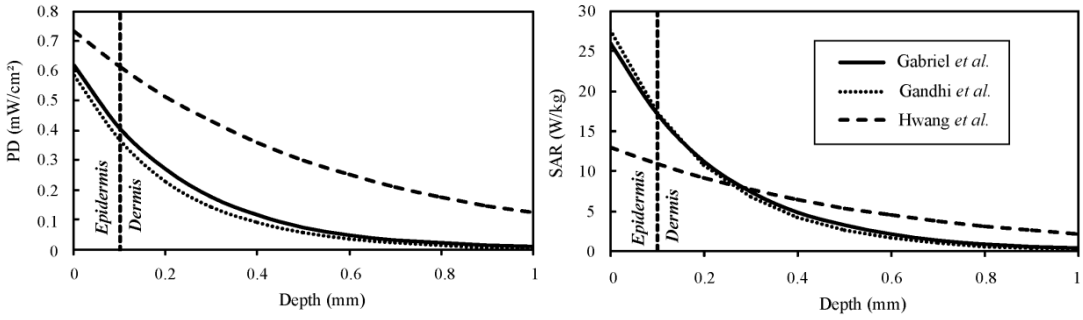


(a) PD (b) SAR

**Figure 2-6**: Attenuation of PD and SAR in the skin for an 1 mW/cm² IPD at 60 GHz [33].

## 2.7 mmW heating

Due to the shallow penetration depth ($\delta_{60GHz} \approx 0.5$ mm), the SAR levels are higher at mmW than at microwaves for the same PD values. Even for low PD significant heating may occur [60]. The relative temperature increase is shown in Figure 2-7 for a normally-incident plane wave at 60 GHz with a PD of 1 mW/cm² and 5 mW/cm², over an average area of 20 cm². These results correspond to the analytical solution of the 1-D heat transfer equation that takes into account the effect of surface cooling and blood flow [46]:

$$\rho c \frac{\partial T'}{\partial t} = k \frac{d^2 T'}{dx^2} - V_s \left( T' - T_0 \right) + Q\left( x,t \right), \tag{3}$$

where $\rho$ (g/cm³) is the tissue density, $c$ (cal/g°C) is the tissue specific heat, $k$ (cal/cm/s°C) is the heat conduction coefficient, $V_s$ (cal/cm³/s°C) is the product of specific blood flow rate, blood density and blood specific heat, $Q(x,t)$ (cal/cm³/s) is the heat deposition from the electromagnetic exposure, $T'(x,t)$ (°C) is the tissue temperature, $T_0$ is the arterial blood temperature.

It should be noted that heating is correlated with the coefficient of the heat transfer from the skin to air. Moreover, the temperature distribution depends on the geometrical and thermal properties of the skin model [22], but it is also related to the blood flow in the skin (i.e. to the environmental temperature and physiological conditions) [29], [31]. It is important to underline that the temperature increments induced by the PD below current international exposure limits are much lower than environmental thermal fluctuations.

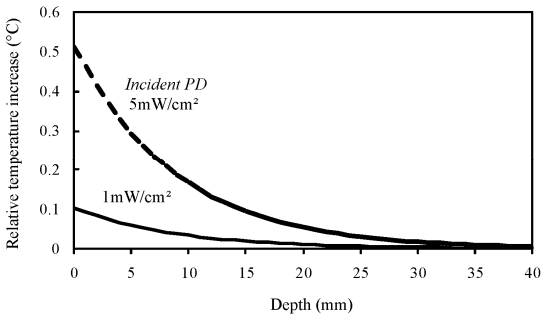


**Figure 2-7**: Temperature increments for a homogeneous skin model exposed to a normally incident plane wave at 60 GHz [33]. The averaging surface area is 20 cm².

## 2.8 Influence of clothing

So far, only limited analytical and numerical data are available in the literature on this topic. In particular, a numerical investigation restricted to the transmission coefficient for a normally-incident plane wave in the presence of a textile is presented in [61], while an analytical solution for normal incidence is provided in [33].

In [33], a plane wave is normally incident to a multilayer structure, in particular a three-layer model (i.e. skin / clothing / air) and a four-layer model (i.e. skin / air gap /clothing / air). Gabriel's data have been used for skin properties (i.e. $\varepsilon^* = 7.98 - j\cdot 10.90$), while $\varepsilon_c = 1.25 + j\cdot 0.024$ for the clothing [62] (this corresponds to dry fleece at microwave frequencies). The transmission coefficient is computed for a typical range of clothing thickness between 0 and 1.2 mm. **As shown in Figure 2-8, the transmission coefficient slightly increases with the clothing thickness. However, the presence of an air gap between clothing and skin induces a decrease of the power transmitted to the skin.**

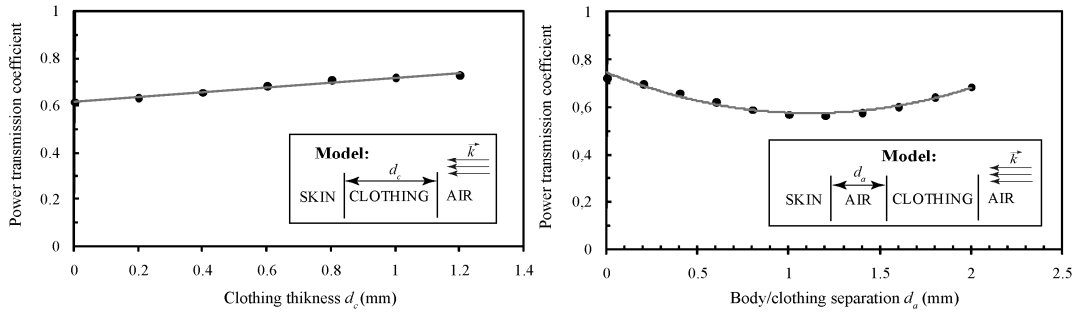


(a) (b)

**Figure 2-8**: Power transmission coefficient at 60 GHz: (a) with / without clothing, (b) as a function of an air gap [33].

## 2.9 Propagation along and around the human body

Applications of mmW technologies in the field of Wireless Body Area Networks (WBANs) have been investigated over the last years. These applications include personal healthcare, entertainment, identification systems, sport, smart home, space, and military applications. It is well known that existing WBANs systems operate around 2.4 GHz or ultra wide band (UWB) spectrum [63-69]. Since they are becoming more congested, increasing the operating frequency in the 60-GHz band seems to be an attractive option. It is also important to underline that, in a WBAN scenario, an essential component of the propagation medium is the human body, since the transmitter (TX), the receiver (RX) or both are placed on the human body surface. WBANs at mmW require careful characterization of the antenna / human body interaction to evaluate the antenna characteristics and human body exposure levels. Indeed, the presence of the antenna in the proximity of the human body may result in significant changes of the antenna input impedance, radiation pattern, antenna efficiency. Moreover, in order to evaluate experimentally the performance of antenna systems, it is necessary to develop appropriate tissue-equivalent phantoms [55]. The latter can be used to quantify the human body exposure levels, as explained in Section 2.4, as well as to investigate the on-body propagation, in a reproducible and controlled manner.

Recent analytical, numerical and experimental studies on WBANs at 60 GHz have been published [56], [57], [70-73]. Some interesting findings are summarized below:

- The path gain between two antennas placed on the body depends on the antenna / body separation distance, as well as on the antenna polarization [56], [72].
- Analytically, the propagation around the human body can be modeled using creeping wave theory [73], [74].
- The received signal is sensitive to the angle of arrival (proper TX-RX alignment is required).
- A line of sight (LOS) channel model is more appropriate [56], [57], [70-75].
- Human body daily activities influence the propagation properties:
    - Attenuation at mmW is much stronger than at microwaves,
    - TX-RX separation distance should be small,
    - Signal fading is caused by shadowing and polarization mismatch.

In an indoor environment, the human body may shadow a significant path between two antennas placed somewhere in the environment, attenuating the signal by about 16 dB [75]. However, this attenuation can be reduced using angular diversity thanks to a proper antenna positioning.

As previously shown in Section 2.8, clothing may influence the propagation. In [57], the path gain along a semi-solid skin equivalent phantom ($\varepsilon^* = 8.11 - j\cdot 11.12$) between two V-band waveguides was analyzed in the presence of textile, and results are shown in Figure 2-9. The path gain variations related to the presence of regular textile (typically 0–5 dB) are lower than the changes of the path gain on a real human body occurring due to the different postures, movements, and positioning of antennas (typically above 10 dB) [70].

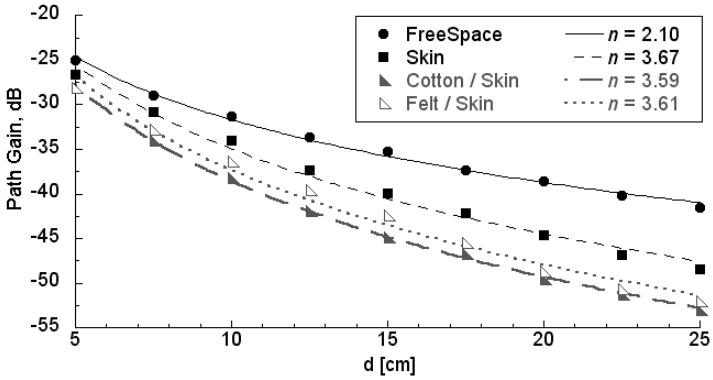


**Figure 2-9**: Path gain at 60 GHz versus separation distance *d* between two open-ended waveguide antennas: in free space, along the skin-equivalent phantom and along the textile / skin phantom [57]. As textiles, 0.2 mm-thick cotton ($\varepsilon_{cotton} = 2 - j\cdot 0.04$) and 2 mm-thick felt ($\varepsilon_{felt} = 1.22 - j\cdot 0.036$) were considered.

# 3. Guidelines for exposure limits

Limits of exposure to EMF are provided by guidelines [4], [5] and standards [6-10] to protect against potential adverse health effects. These limits are intended to apply to all human exposures except exposure of patients undergoing procedures for diagnosis or treatment. They apply to both occupational and public exposure (see definitions on page 8).

At mmW, the human body becomes electrically very large (typically $1150\lambda_g$ for an average adult, i.e. 1.75 m height and 70 kg); the EMF is absorbed at the body surface and the dosimetric quantity used at these frequencies is IPD.

In the following, the generally-used regulations are reviewed, and the exposure limits are provided. **It is important to note that current recommendations do not provide any recommendations for near-field exposures and only deal with far-field exposures at mmW.**

## 3.1 ICNIRP

The basic restrictions (BRs) and reference levels (RLs) recommended by ICNIRP are the following:

**Table 3.1**: BRs for occupational and general public for 10 - 300 GHz frequency range [4].

| Public exposure | Power density ($mW/cm^2$) | Averaging surface ($cm^2$) | Averaging time (min) |
|---|---|---|---|
| Occupational | 5 | 20 | $68/f^{1.05}$ |
| | 100 | 1 | |
| General | 1 | 20 | |
| | 20 | 1 | |

**Table 3.2**: RLs for occupational and general public for 2 - 300 GHz frequency range [4].

| Public exposure | E-field (V/m) | H-field (A/m) | B-field (μT) | Power density PD ($mW/cm^2$) |
|---|---|---|---|---|
| Occupational | 137 | 0.36 | 0.45 | 5 |
| General | 61 | 0.16 | 0.20 | 1 |

**N.B.** - The general public restrictions for PD are lowered by a factor of 5 compared to occupational exposure conditions.

- The averaging surface area of 20 $cm^2$ is the surface area of a cube with edge dimension 1.8 cm (see Section 4.4 for more details).

- Thermal effects of the cornea (which surface area is ~1 $cm^2$) were used to establish the localized exposure limits to mmW (i.e. 20 $mW/cm^2$ for general public and 100 $mW/cm^2$ for occupational public).

- The maximum power densities averaged over 1 $cm^2$ should not exceed 20 times the values averaged over 20 $cm^2$.

- In Table 3.2 the power densities are averaged over 20 $cm^2$.

- For frequencies exceeding 10 GHz, the RLs $E^2$, $H^2$, $B^2$ and $PD$ are to be averaged over $68/f^{1.05}$ - min period of time ($f$ – frequency in GHz).

- At 60 GHz the averaging time is approximately 1 min.

## 3.2 IEEE

The IEEE standardization expresses the recommendations in terms of *Basic restrictions (BRs)* and *Maximum permissible exposure values (MPE)*. For frequencies between 3 GHz and 300 GHz, the *BRs* and *MPE* are the same.

**Table 3.3**: MPE for occupational and general public for whole-body exposure in the 30 – 300 GHz frequency range [10].

| Public exposure | Power density ($mW/cm^2$) | Averaging surface ($cm^2$) | Averaging time (min) |
|---|---|---|---|
| Occupational | 10 | 100 | $25.24/f^{0.476}$ |
| | 100 | 1 | |
| General | 1 | 100 | |
| | 100 | 1 | |

Localized exposure is considered when the exposed area is less than 1/20 of the total projected area of the body (i.e. 10 000$cm^2$ cross-section of the human body, 100 $cm^2$ human hand/face).

**Table 3.4**: Local exposure in the 30 – 300 GHz frequency range [10].

| Public exposure | Power density ($mW/cm^2$) | Averaging surface ($cm^2$) | Averaging time (min) |
|---|---|---|---|
| Occupational | $20(f/3)^{0.2}$ | 1 | $25.24/f^{0.476}$ |
| General | 20 | | |

**N.B.** – $f$ is the frequency in GHz. At 60 GHz the averaging time is 3.6 min.

## 3.3 CENELEC

The European Union included the limit values and physical quantities from the ICNIRP guidelines in two main EU documents: the European Recommendation for general population 1999/519/EC [6] and the Directive of the European Parliament and of the Council, 2004/40/EC [7].

The basic restrictions, given in Table 3.5, are set so as to account for uncertainties related to individual sensitivities, environmental conditions, and for the fact that the age and health status of members of the public vary.

**Table 3.5**: BRs for occupational and general public in the 2-300 GHz frequency range [8].

| Public exposure | Power density ($mW/cm^2$) | Averaging surface ($cm^2$) | Averaging time (min) |
|---|---|---|---|
| Occupational | 5 | 20 | $68/f^{1.05}$ |
| | 100 | 1 | |
| General | 1 | 20 | |
| | 20 | 1 | |

**Table 3.6**: RLs for occupational and general public in the 2-300 GHz frequency range [8].

| Public exposure | E-field (V/m) | H-field (A/m) | B-field (μT) | Power density *PD* (mW/cm$^2$) |
|---|---|---|---|---|
| Occupational | 137 | 0.36 | 0.45 | 5 |
| General | 61 | 0.16 | 0.20 | 1 |

**N.B.** - The maximum power densities averaged over 1 cm$^2$ should not exceed 20 times the values averaged over 20 cm$^2$ in Table 3.6.

- For frequencies exceeding 10 GHz, the RLs $E^2$, $H^2$, $B^2$ and *PD* are to be averaged over $68/f^{1.05}$ - min period of time ($f$ – frequency in GHz) (@ 60 GHz the averaging time ≈ 1 min).

Most Member States have adopted the EU Recommendation and some have imposed obligatory measures to control EMF exposure of the general public. Although most of them consider the EU Recommendation sufficient to provide a high level of health protection, some have adopted more stringent exposure limits. In [9], the European Commission verified the application of 1999/519/EC recommendation by the EU Member States. Table 3.7 summarizes the BRs and RLs implemented by different states.

**Table 3.7**: Summary of the implemented Council Recommendation 1999/519/EC levels in Member States related to BRs and RLs in [9].

| Country | Stricter levels than in EU Recommendation | | Same levels than in EU Recommendation | | Less stricter levels than in EU Recommendation | |
|---|---|---|---|---|---|---|
| | BRs | RLs | BSs | RLs | BRs | RLs |
| AT | | | X | X | | |
| BE | X[a] | X[a] | | | | |
| BG | | X | X | | | |
| CH | | X | X | | | |
| CZ | | | X | X | | |
| CY | | | | X | X | |
| DE | | | | X | X | |
| DK | | | | | X | X |
| EE | | | | X | ? | |
| ES | | | X | X | | |
| FI | | | X | X | | |
| FR | | | X | X | | |
| GR | X[a] | X[a] | | | | |
| HU | | | X | X | | |
| IE | | | | X | X | |
| IT | | X | X | | | |
| LT | | X | | | X[b] | |
| LU | | X | X | | | |
| LV | | | X | X | | |
| MT | | | X | X | | |
| NL | | X[a] | | | X | |
| PL | | X | | | X | |
| PT | | | X | X | | |
| RO | | | X | X | | |
| SE | | | X | X | | |
| SI | | X | | | X | |
| SK | | | | X | X | |
| UK | | | X | X | | |

a) Not for the whole frequency range — b) Only for workers

**Particularities for BRs**:

- Greece: applies reduction factors of 60 - 70% for all land-based antennas (60% when antennas are located at less than 300 m from schools, kindergartens, hospitals or eldercare facilities).
- Italy: values are 10 times lower for PD (applicable to power plants and fixed telecommunication equipment).

**Particularities for RLs:**

- Bulgaria: different zones are identified: (1) zones where human exposure is rare or practically impossible where higher limit values are applied; (2) zones with continuous exposure where much lower limits are set; (3) areas for sensitive groups (including children, pregnant women, elderly and ill people) where much lower limits are set.
- Slovenia: applies 10 times more stringent RLs for radiation sources in sensitive areas (e.g. schools, day-care centers, hospitals, residential housing, etc).
- Greece: the RLs of the Recommendation were set as the safety limits for ELF fields, while new reference levels have been derived for all land-based antennas in the frequency range of 1 kHz to 300 GHz.
- Lithuania: from 300 MHz to 300 GHz even 100 times restriction factor applies (i.e. 0.01 $mW/cm^2$).
- Switzerland: the general exposure limits comply with the RLs in the Recommendation; additional precaution factors of 10 to 100 are applied for single installations in “sensitive areas”. Additional safety measures are applied for mobile telecommunication stations, radio and TV broadcasting stations and for high-voltage power lines.

# 4. Exposure limits – Considerations

The exposure limits recommended by ICNIRP, IEEE and CENELEC have been established by considering scientific literature data. In the following, the most important ones are reviewed, and some important points regarding the mmW radiations are summarized.

## 4.1 Whole-body resonance

Generally, the limits for RLs / MPEs are based on recommendations of field strength or of plane-wave equivalent power densities of the incident fields. These limits are based on well-established findings from the literature, which showed that human body, as a whole, exhibits frequency-dependent rates of EMF absorption [76]-[78]. Whole-body-averaged SAR values approach maximal values when the long axis of the body is parallel to the E-field vector and is four tenths of a wavelength of the incident field. At 2.45 GHz ($\lambda$ = 12.5 cm), a standard man (long axis = 175 cm) will absorb about half of the incident energy. Maximum absorption occurs at a frequency near 70 MHz for standard man (height = 1.75 m, weight = 70 kg), which defines the whole-body resonance (Figure 4-1). The whole-body resonance values for the range of human body size become relatively flat for frequencies in the range of about 1 to 3 GHz. The recommended RLs / MPEs have been developed to reflect whole-body resonance and SAR frequency dependence.

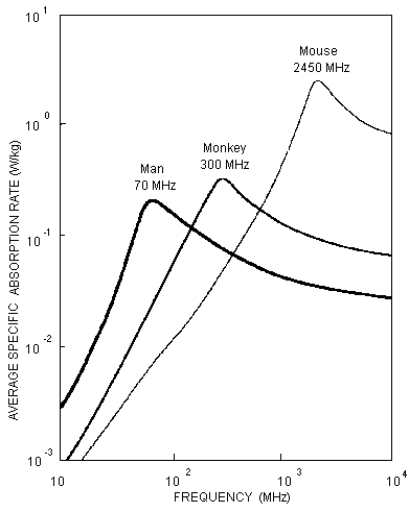


**Figure 4-1**: Average SAR for three different species including an average human man (1.75 m height and 70 kg weight) exposed to 1 mW/cm$^2$ PD with E-field vector parallel to the long axis of the body [79].

**Above 10 GHz, the absorption is quasi-optical and body resonance considerations do not apply. At mmWs, the penetration depth is less than 1 mm.**

## 4.2 Temperature considerations

**The rational to establish the limits of the BRs at mmW for local exposure relies on scientific publications on temperature increase in the eye and the potential adverse health effects caused by this increase. The temperature threshold in the eye was established at 41°C (corresponds to a temperature increase of about 3-4°C), over which cataract formation may appear.**

It was noticed that the maximum eye temperature increase (~4°C for a SAR of 10 W/kg at 2.45 GHz [17]) in near-field and far-field exposures is below the temperature threshold (41°C), and does not produce any adverse effects.

**For skin tissue exposure at mmWs, the current literature showed that exposure at the recommended limits (for the corresponding averaging surface area, i.e. 20 $cm^2$ and 1 $cm^2$) will probably not increase its temperature by as much as 1°C.**

## 4.3 Time considerations

Generally, the standards have used 6 min averaging time corresponding to a time constant for partial body heating for frequencies below 10 GHz.

For frequencies above 10 GHz, the averaging time corresponds to:

- **$68/f^{1.05}$** (CENELEC, ICNIRP) which corresponds to about 0.92 min at 60 GHz, 0.74 min at 74 GHz, and 0.65 min at 84 GHz.
- a less restrictive value recommended by IEEE, in particular **$25.24/f^{0.476}$** which corresponds to about 3.6 min at 60 GHz, 3.25 min at 74 GHz, and 3.06 min at 84 GHz.

## 4.4 Spatial considerations

For non-uniform illumination there is a possibility that the whole-body average field exposure does not exceed the BRs, but still results in excessive local heating.

The rationale to establish the averaging surface area in the exposure level recommendations are the following:

- **20 $cm^2$** is the surface area of a cube with edge dimension of 1.8 cm. This averaging dimension is related to the human eye, where biological effects like cataract have been noticed at microwave frequencies. The eye dimensions differ among adults by 1-2 mm. At birth, the eye is about 1.6-1.7 cm diameter. At 13 years old, the eye attains the full size, from anterior to posterior a diameter of about 2.4 cm, a volume of about 6 $cm^3$ and a mass of 7.5 g [80].
- **1 $cm^2$** is the surface area of the cornea, where some effects like cataract may appear.
- The IEEE recommendations are less restrictive, and an averaging surface are of **100 $cm^2$** is considered, which corresponds to the surface of human face / hand area.

## 4.5 Volume considerations

As previously said, the EMF exposure results in adverse health effects only when the exposure results in a harmful temperature increase. At microwaves, SAR has been correlated with the temperature increase. However, the SAR averaged over a particular volume is not always proportional with temperature increase. Indeed, the temperature increase depends on the size of the region absorbing energy, blood flow and other factors. If a small area is heated, the heat is transferred rapidly to cooler areas, so its temperature does not increase significantly. If a larger area is heated, the rapid local heat transfer produces a uniformly elevated temperature through the area. The volume size is sufficiently small to avoid excessive temperature increases, but large enough to get an averaged SAR which corresponds to the real temperature increase.

Another parameter that provides a reasonable reference for the volume that can be heated is the penetration depth of RF energy. The latter decreases when the frequency increases. For example, at 3 GHz, the penetration depth in muscle or other tissues is about 2 cm. This dimension was considered to distinguish two regions: below 3 GHz where heating is uniform over a few centimeter areas, and above 3 GHz where heating is limited to the superficial layers (i.e. skin) and highly non-uniform in depth tissues. At frequencies of 3 GHz and below, a cube of 2.15 cm side (volume about 10 $cm^3$) is sufficiently large to obtain an average SAR that ensure a temperature

increase uniformly distributed over this volume. Above 3 GHz, this volume is less suitable for averaging due to the temperature gradients that occurs in correspondence to reduced penetration depth.

**Dosimetric quantity used by regulations at mmW (where the penetration depth is small) is power density and not SAR. The latter, can however be used as intermediate parameter to retrieve the incident and in-tissue PD.**

# 5. Numerical study on plane wave exposure in V- and E-bands

As previously introduced in Section 2, due to the shallow penetration at mmW, the interaction with the human body is limited to the skin. It has been demonstrated that, at 60 GHz, a homogeneous skin model can be used instead of a multilayer model [55]. Since in E-band the penetration is even less than at 60 GHz, a homogeneous model can be used as well. Plane waves in V- and E-bands illuminating a semi-infinite rectangular phantom with the dry skin dispersive dielectric properties provided by Gabriel's data are considered here.

## 5.1 Skin dielectric properties in the 57-86 GHz range

The dry skin dielectric properties are summarized in Table 5.1 for some particular frequencies in the 57-86 GHz range.

**Table 5.1**: Skin dielectric properties [38].

| Frequency, *f* (GHz) | ε' | tanδ | ε*=ε' - *j*·ε" |
|---|---|---|---|
| 57 | 8.34 | 1.36 | 8.34 - j·11.34 |
| 60 | 7.98 | 1.37 | 7.98 - j·10.90 |
| 66 | 7.37 | 1.37 | 7.37 - j·10.10 |
| 71 | 6.96 | 1.37 | 6.96 - j·9.54 |
| 74 | 6.75 | 1.36 | 6.75 - j·9.18 |
| 76 | 6.63 | 1.36 | 6.63 - j·9.02 |
| 81 | 6.34 | 1.35 | 6.34 - j·8.56 |
| 84 | 6.19 | 1.34 | 6.19 - j·8.29 |
| 86 | 6.10 | 1.33 | 6.10 - j·8.11 |

## 5.2 Numerical model and assumptions

The simulations were performed using CST Microwave Studio® software. In order to generate a plane wave with different incidence angles, a Floquet port above a homogenous model and periodic boundary conditions were used (Figure 5-1).

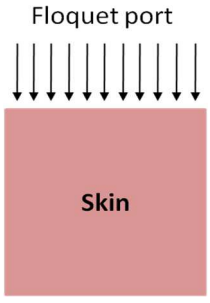


**Figure 5-1**: Numerical model.

Both parallel (TM mode: $\vec{E}$ field is parallel to the plane of incidence) and perpendicular (TE mode: $\vec{E}$ field is perpendicular to the plane of incidence) polarizations were analyzed (see Figure 2-4). The reflection and transmission power coefficients were calculated for three frequency bands: 57-

66 GHz, 71-76 GHz and 81-86 GHz. The corresponding dielectric properties of skin were considered for these frequencies according to Table 5.1.

## 5.3 Numerical results – V-band

Figure 5-2 represents the power reflection and transmission coefficients for both perpendicular and parallel polarizations in V-band. At 57, 60 and 66 GHz, the differences are insignificant. For normal incidence, approximately 38% of the incident power is reflected by the skin. It should also be noticed that transmission in the skin is higher for parallel polarization.

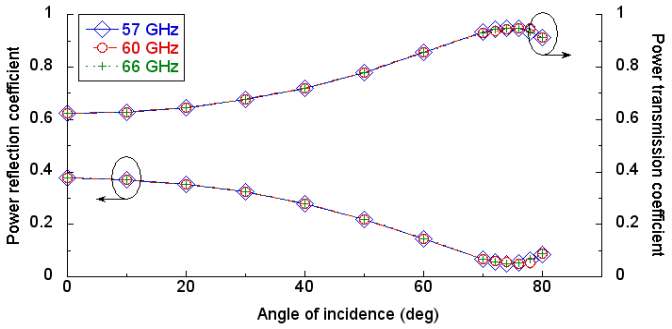


(a)

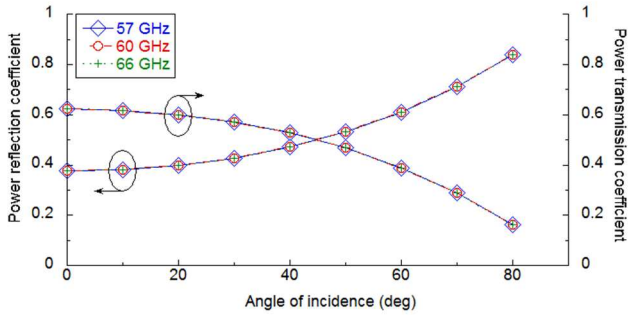


(b)

**Figure 5-2**: Power reflection and transmission coefficients in V-band for: (a) parallel (TM) polarization and (b) perpendicular (TE) polarization.

## 5.4 Numerical results – E-band

The differences in terms of reflection and transmission coefficients are insignificant in the 71-76 GHz interval (Figure 5-3), as in the V-band case. Moreover, for normal incidence, the reflected power decreases compared to V-band and is around 35%.

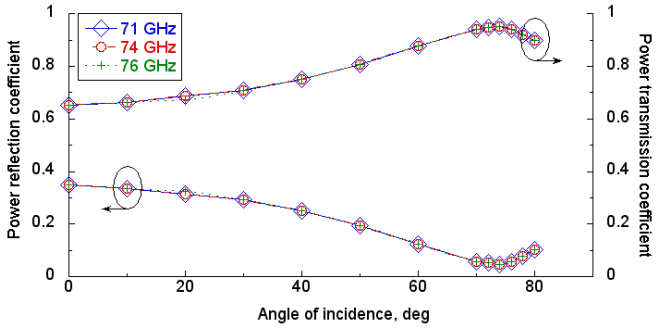


(a)

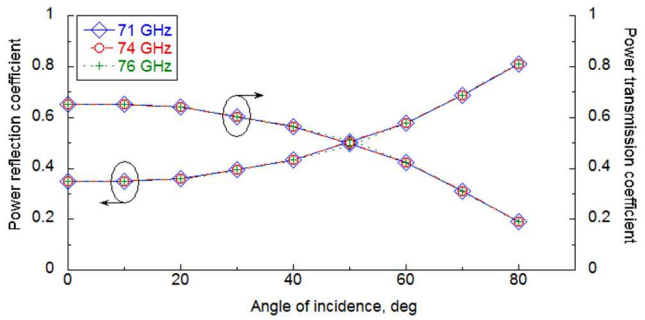


(b)

**Figure 5-3**: Power reflection and transmission coefficients in E-band (71-76 GHz) for: (a) parallel (TM) polarization and (b) perpendicular (TE) polarization.

As expected, the differences in terms of reflection and transmission are insignificant in the 81-86 GHz band (Figure 5-4). Under normal incidence, 32% of the incident power density is reflected from the skin.

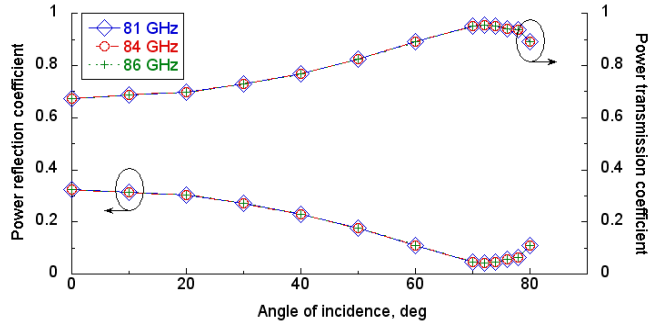


(a)

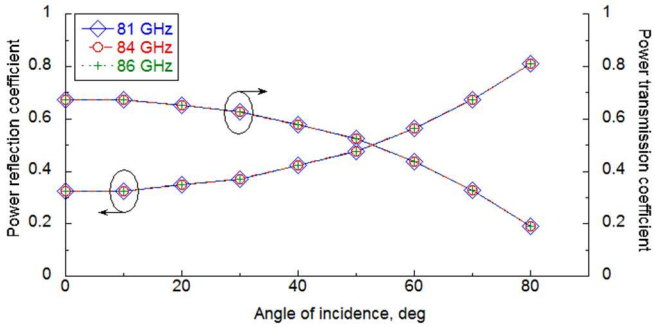


(b)

**Figure 5-4**: Power reflection and transmission coefficients in E-band (81-86 GHz) for: (a) parallel (TM) polarization and (b) perpendicular (TE) polarization.

As previously noted for V-band, the transmission in the E-band is stronger for parallel polarization compared to the perpendicular polarization.

Figure 5-5 represents the power reflection and transmission coefficients at normal incidence over the 50-90 GHz band. It is noticed that power reflection coefficient decreases with frequency, while the transmission increases.

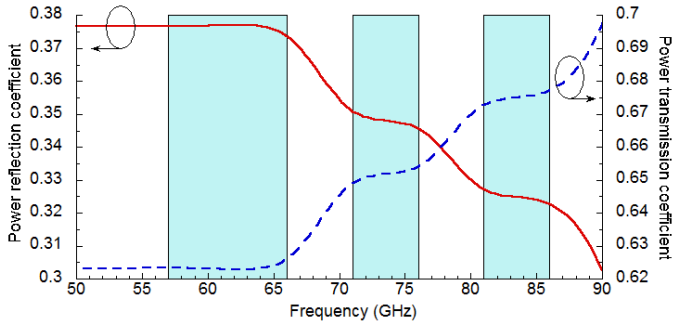


**Figure 5-5**: Power reflection and transmission coefficients in the 50-90 GHz at normal incidence.

Figure 5-6 presents the power reflection and transmission coefficients at 60, 74 and 84 GHz for both polarizations (TM and TE). As previously noted, the transmission coefficient increases when frequency increases.

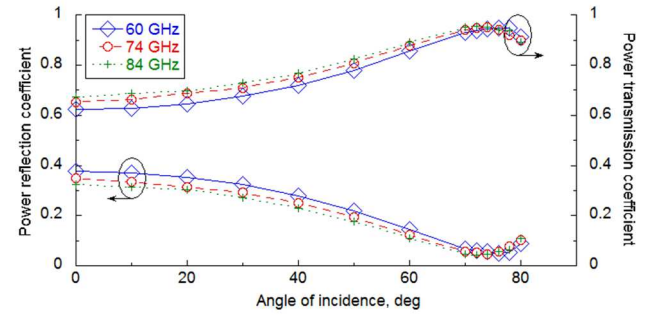


(a)

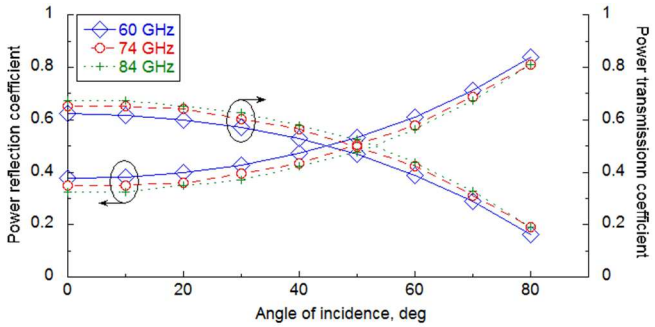


(b)

**Figure 5-6**: Power reflection and transmission coefficients at 60-74-84 GHz for: (a) parallel (TM) polarization and (b) perpendicular (TE) polarization.

## 5.5 Power density attenuation

Figure 5-7 shows the attenuation of the PD at different frequencies calculated according to equation (2) for normal incidence. It is shown that the transmitted power decreases exponentially in the skin as a function of depth. Maximum PD occurs at the surface; the corresponding values are summarized in Table 5.2.

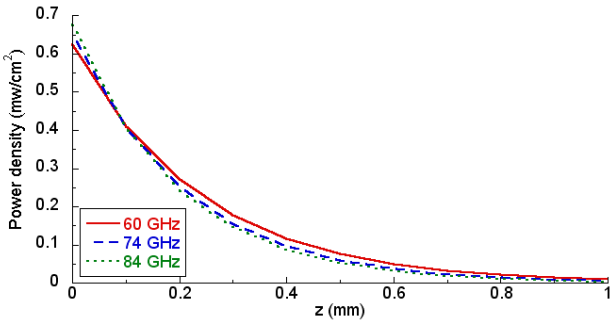


(a)

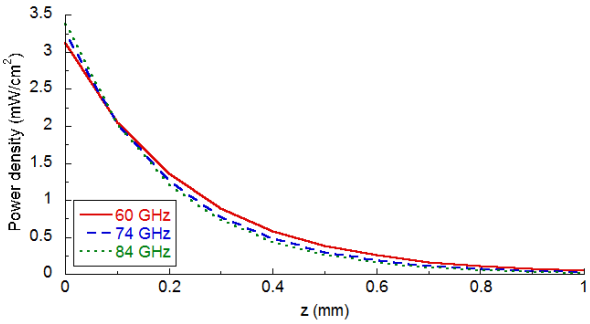


(b)

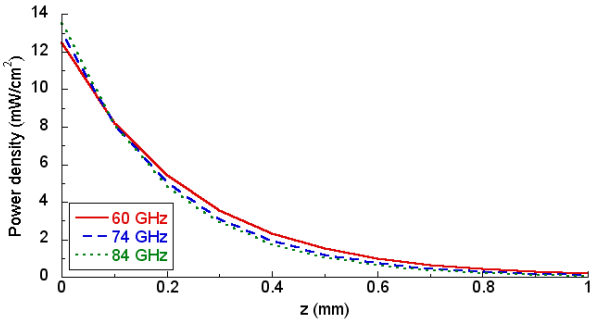


(c)

**Figure 5-7**: Attenuation of the PD in the skin at 60-74-84 GHz, normal incidence, and for an incident PD of: (a) 1 mW/cm$^2$, (b) 5 mW/cm$^2$ and (c) 20 mW/cm$^2$.

**Table 5.2**: Penetration depth, power reflection coefficient and maximum PD in the skin for an incident PD of 1 mW/cm$^2$, 5 mW/cm$^2$ and 20 mW/cm$^2$.

| **Frequency *f* (GHz)** | **Penetration depth *δ* (mm)** | **Power transmission coefficient *%*** | **Max power density *PD* (mW/cm²)** | | |
|---|---|---|---|---|---|
| | | | **@ 1 mW/cm²** | **@ 5 mW/cm²** | **@ 20 mW/cm²** |
| 60 | 0.48 | 62 | 0.62 | 3.12 | 12.5 |
| 74 | 0.42 | 65 | 0.65 | 3.26 | 13.0 |
| 84 | 0.39 | 68 | 0.68 | 3.38 | 13.5 |

**To summarize:**

- **30-38% of the incident power is reflected at the air / skin interface for normal incidence in the 50-90 GHz frequency band. Power reflection coefficients deviate significantly from the normal incidence values, if oblique incidence is considered.** Transmission in the skin is higher for parallel (TM) polarization than for perpendicular (TE) polarization.
- **Maximum power density occurs at the skin surface. Transmitted power decreases nearly exponentially in the skin as a function of depth.**
- **The maximum deviations found over the 57-86 GHz range are the following: (1) 2.18 % in terms of the power transmission coefficient; (2) 2 % in terms of the peak power density in the skin.**

# 6. Numerical modelling at mmW frequencies

Finite Difference Time Domain Technique (FDTD) [81] and Finite Integrated Technique (FIT) [82] are numerical analysis methods widely used in computational electromagnetic fields. They are based on the discretization of Maxwell equations in time domain and are the most preferred techniques to determine the specified SAR / PD levels.

Their application at mmW might become limited due to electrically large dimensions of the entire human body. The investigated volume would require a discretization with cubic cells of $\lambda/10$ dimensions, and as a consequence, the number of cells would be very large (e.g. ~$10^{10}$). In this case, the computational resources, even with parallelization / symmetry would be far prohibitive. A solution for dosimetry is to use only some body parts, for instance the head and the hand for user's exposure to mobile devices.

When propagation and scattering involve electrically-large objects (i.e. entire human body), high-frequency asymptotic techniques are computationally efficient and provide accurate solutions. Recently, considerable attention has been dedicated to ray-tracing based techniques to investigate the effect of the human body presence in an indoor propagation scenario [75] or in on-body applications [83], [84]. However, in the available ray-tracing tools some limitations should be taken into account: modification of the antenna radiation pattern in proximity of the human body, propagation through the clothing layers, proper definition of the human body tissues, as well as the clothing.

Numerical phantoms make use of MRI images of various organs and different tissues of real human body. The most used phantoms are the *volumetric phantoms* (Figure 6-1), which can be discretized into voxels, with a resolution of 1 $mm^3$. However, the applicability of these detailed phantoms at mmW is limited because of the shallow penetration depth.

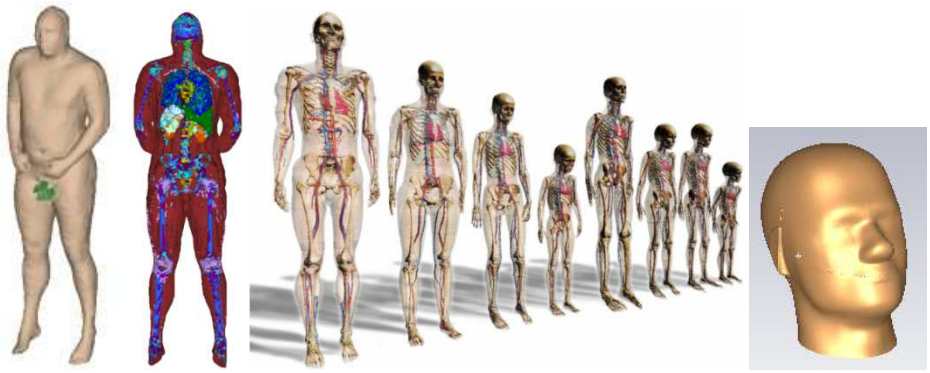

(a) (b) (c)

**Figure 6-1**: Volumetric human phantoms: (a) Hugo model [84], (b) Virtual Family [86], (c) SAM [85].

During the years, wireless personal communications and in particular cellular mobile phones, wireless local area networks and more recently body-area networks have raised public concerns on potential health effects due to electromagnetic fields exposure. Numerical results on dosimetry, antenna / human body interaction and propagation have been provided at microwaves [16, 18-19], and more recently at mmWs [25-30, 34], with computational results for whole-body average and local SAR, as well as for power density [61-70] (see sections 2.1, 2.2 and 2.9). Also, results of the human body effect on the device / antenna have been presented in terms of antenna mismatch, radiation patterns, and efficiency [63, 67-68]. It was shown that, when placed on or in close proximity

to the human body, antennas experience detuning, radiation pattern distortion, efficiency reduction. In order to minimize the human body effect on the antenna performance, the latter should be designed to operate properly in close proximity to the human body.

# 7. Conclusion

The report describes the most important aspects of the mmW interactions with the human body in terms of reflection, transmission and power absorption. The ICNIRP guidelines and IEEE, CENELEC standards are reviewed, as well as the most recent aspects of mmW dosimetry.

The numerical analysis performed in V- and E-bands, provides a preliminary overview on the interaction mechanism between a far-field exposure source (plane wave) and the human body. The results confirm the previous findings, in particular that the maximum power density occurs at the skin surface. The transmitted power decreases exponentially in the skin as a function of depth. At 1 mm depth under the skin surface, the absorbed power is attenuated by more than 98% (see Figure 5-7). This finding suggest that, a few mm-thick homogenous skin layer is sufficient for numerical and experimental modeling.

In V-band the transmission is about 62 %, and increases in E-band to about 68% for normal incidence. Transmission in the skin depends on the polarization and angle of incidence. Indeed, for parallel (TM) polarization higher values occur than for perpendicular (TE) polarization.

# 8. Future work

A more realistic dosimetry study will be performed in Task 4.5. In particular, the study and analysis of exposure levels induced in the most exposed parts of the human body under a representative use case at 60 GHz will be investigated. Numerical analysis will be conducted preferably using the commercial software CST Microwave Studio®.

A first scenario will include the human body exposure to one or several Access Points (AP) (Figure 8-1). This scenario will be analytically investigated together with Orange partner. The analysis will be based on AP data (radiated power, antenna gain, distance to the user), and the expected output results will be presented in terms of power density, E-field, SAR. Moreover, for the downlink scenario an alternative approach will be address to estimate the IPD needed to get a reliable QoS between the AP and the user.


**Figure 8-1**: Access point – user case scenario.

The second scenario will include the user exposure to the mobile terminal (used as a near-field radiation source). The following terminal positions defined by CEA will be considered (Figure 8-2):

- Phone call position: terminal against users ear,
- Browsing position: terminal in front of the user.

(a) (b)

**Figure 8-2**: Terminal positions: (a) phone call; (b) browsing.

The following action points are planned:

- A comparison between HFSS and CST regarding the antenna module will be performed. Return loss and radiation patterns will be compared.
- The possibility of using a simplified antenna module with representative radiation characteristics (boresight radiation pattern with maximum gain of 10 dBi, Front to Back ratio >14 dB, and HPBW: 36° (E-plane) and 64° (H-plane)) will be analyzed. In particular, the possibility to remove the electronic part and terminal will be taken into consideration.
- The human body will be modelled as a homogeneous layer with skin dielectric properties assigned (@ 60 GHz $\varepsilon^* = 7.98 - j \cdot 10.90$). The possibility of removing some body parts will be analyzed.
- The following module positions in the terminal will be considered: upper right / left corner and top edge:

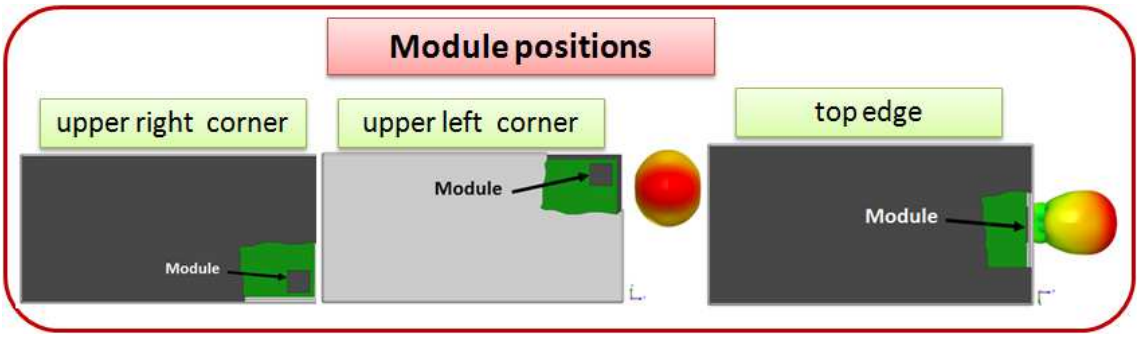


**Figure 8-3**: Module positions in the terminal box.

- Parametric analysis varying the terminal to the user's ear distance, and distance / position of the mobile terminal with respect to the human body will be performed.

Peak / average values of the $|E|$ field intensity at the skin surface, power density and SAR will be provided

- for the recommended exposure limits:
  - General public: 1 mW/cm$^2$ averaged over 20 cm$^2$, and 20 mW/cm$^2$ averaged over 1 cm$^2$.
  - Occupational public: 5 mW/cm2 averaged over 20 cm$^2$, and 100 mW/cm$^2$ averaged over 1 cm$^2$.
- for the transmitted power of the terminal (as provided by D1.2).

The possibility to use an equivalent incident power density, for near-field exposures, will be evaluated.

Also, in the frame of Task4.5, a study regarding the local exposure to 100 mW/cm$^2$ averaged over a surface area of 1 cm$^2$ will be performed. So far, only far-field exposure has been investigated (see Section 2.7), and results have been provided for the recommended limit values of 1 mW/cm$^2$ and 5 mW/cm$^2$ averaged over 20 cm$^2$ (see Figure 2-7).

# 9. References


[1] T. Baykas, C.S. Sum, Z. Lan, J. Wang, M.A. Rahman, and H. Harada, "IEEE 802.15.3c: The first IEEE wireless standard for data rates over 1 Gb/s", *IEEE Commun. Mag.*, vol. 49, no. 7, pp. 114-121, Jul. 2011.

[2] J. Wells, "Faster than fiber: the future of multi Gb/s wireless", *IEEE Microw. Mag.*, vol. 10, no. 3, pp. 104-112, May 2009.

[3] R.C. Daniels, J.N. Murdock, T.S. Rappaport, and R.W. Heath, "60 GHz wireless: up close and personal", *IEEE Microw. Mag.*, vol. 11, no. 7, pp. 44-50, Dec. 2010.

[4] ICNIRP: "Guidelines for limiting exposure to time-varying electric, magnetic, and electromagnetic fields (up to 300 GHz)", *Health Physics*, vol. 74, no. 4, pp. 494-522, 1998.

[5] ICNIRP: "Exposure to high frequency electromagnetic fields, biological effects and health consequences (100 kHz - 300 GHz)", ISBN 978-3-934994-10-2, 2009.

[6] 1999/519/EC, "Council recommendation of 12 July 1999 on the limitation of exposure of the general public to electromagnetic fields (0 Hz to 300 GHz)".

[7] 2004/40/EC, "Directive of the European Parliament and of the Council of 29 April 2004 on the minimum health and safety requirements regarding the exposure of workers to the risk arising from physical agents (electromagnetic fields)".

[8] EN 50413 – 2008, "Basic standard on measurement and calculation procedures for human exposure to electric, magnetic and electromagnetic fields (0 Hz – 300 GHz)".

[9] EN 532 – 2008, "Report from the commission on the application of council recommendation of 12 July 1999 (1999/519/EC) on the limitation of the exposure of the general public to electromagnetic field (0 Hz to 300 GHz)".

[10] IEEE Standard for safety levels with respect to human exposure to radio frequency electromagnetic fields, 3 kHz to 300 GHz, ISBN 0-7381-4835-0 SS95389, Apr. 2006.

[11] A.F. Emery, P. Kramar, A.W. Guy, and J.C. Lin, "Microwave induced temperature rises in rabbit eye in cataract research", *J. Heat Transfer*, vol. 97, no. 1, pp. 123-128, Feb. 1975.

[12] A.W. Guy, J.C. Lin, P.O. Kramar, and A.F. Emery, "Effect of 2450 MHz radiation on the rabbit eye", *IEEE Trans. Microw. Techn.*, vol. MTT-23, no. 6, Jun. 1975.

[13] S. Baranski and P. Czerski, "Biological effects of microwaves", *Stroudsburg, PA: Dowden*, pp. 146-149, 1976.

[14] R.D. McAfee, R. Ortiz-Lugo, R. Bishop, and R. Gordon, "Absence of deleterious effects of chronic microwave radiation on the eye of rhesus monkeys", *Ophthalmology*, vol. 90, no. 10, pp. 1243-1245, Oct. 1983.

[15] J.J. Lagendijk, "A mathematical model to calculate temperature distributions in human and rabbit eyes during hyperthermic treatment", *Phys. Med. Biol.*, vol. 27, no. 11, pp. 1301-1311, Nov. 1982.

[16] C. Buccella, V. De Santis, and M. Feliziani, "Prediction of temperature increase in human eyes due to RF sources", *IEEE Trans Electromagn. Compat.*, vol. 49, no. 4, pp. 825–833, Nov. 2007.

[17] NRPB, "Consultation document — Proposals for limiting exposure to electromagnetic fields (0–300GHz)", National Radiological Protection Board, Chilton, Didcot, OX11 0RQ, 185, U.K., May 2003.

[18] P. Bernardi, M. Cavagnaro, S. Pisa, and E. Piuzzi, "SAR distribution and temperature increase in an anatomical model of the human eye exposed to the field radiated by the user antenna in a wireless LAN", *IEEE Trans. Microw. Theory Tech.*, vol. 46, no. 12, pp. 2074-2081, Dec. 1998.

[19] A. Hirata, S. Matsuyama, and T. Shiozawa, "Temperature rises in the human eye exposed to EM waves in the frequency range 0.6 – 6 GHz", *IEEE Trans Electromagn. Compt.*, vol. 42, no. 4, pp. 386-393, Nov. 2000.

[20] A. Hirata, "Temperature increase in human eyes due to near-field and far-field exposures at 900 MHz, 1.5GHz, and 1.9 GHz", *IEEE Trans. Electromagn. Compt.*, vol. 47, no. 1, pp. 68-76, Feb. 2005.

[21] M. Kojima, M. Hanazawa, Y. Yanashiro, H. Sasaki, S. Watanabe, H. Taki, Y. Suzuki, A. Hirata, Y. Kamimura, and K. Sasaki, "Acute ocular injuries caused by 60 GHz millimeter-wave exposure", *Health Phys.*, vol. 97, no. 3, pp. 212-218, Sep. 2009.

[22] A. Kanezaki, A. Hirata, S. Watanabe, and H. Shirai, "Parameter variation effects on temperature elevation in a steady-state, one-dimensional thermal model for millimeter wave exposure of one- and three-layer human tissue", *Phys. Med. Biol.*, vol. 55, pp. 4647-4659, Jul. 2010.

[23] M. Kojima, H. Sasaki, K. Sasaki, T. Sakai, K. Wake, S. Watanabe, Y. Kamimura, A. Hirata, Y. Suzuki, and M. Taki, "Investigation of acute ocular injury threshold by 76 GHz band exposure in rabbits", *General Assembly and Scientific Symposium - XXX$^{th}$ URSI*, Aug. 2011.

[24] H.A. Kues, S.A. D'Anna, R. Osiander, W.R. Green, and J.C. Monahan, "Absence of ocular effects after either single or repeated exposure to 10 mW/cm$^2$ from a 60 GHz CW source", *Bioelectromagn.*, vol. 20, no. 8, pp. 463-473, Dec. 1999.

[25] F. Gustrau and Achim Bahr, "W-band investigation of material parameters, SAR distribution, and thermal response in human tissue", *IEEE Trans. Microw. Theory Techn.*, vol. 50, no. 10, pp. 2393-2400, Oct. 2002.

[26] A. Papaioannou and T. Samaras, "Numerical model of heat transfer in the rabbit eye exposed to 60 GHz millimeter wave radiation", *IEEE Trans. Biomed. Eng.*, vol. 58, no. 9, pp. 2582-2588, Sept. 2011.

[27] A. Karampatzakis and T. Samaras, "Numerical modeling of heat and mass transfer in the human eye under millimeter wave exposure", *Bioeletromagn.*, vol. 34, pp. 291-299, May 2013.

[28] F.A. Duck, "Physical properties of tissues", *Academic Press*, Bath, UK, ISBN 0122228006, 1990.

[29] S.I. Alekseev and M.C. Ziskin, "Millimeter-wave absorption by cutaneous blood vessels: a computational study", *IEEE Trans Biomed. Eng.*, vol. 56, no. 10, pp. 2380-2388, Oct. 2009.

[30] S.I. Alekseev and M.C. Ziskin, "Enhanced absorption of millimeter wave energy in murine subcutaneous blood vessels", *Bioeletromagn.*, vol. 32, pp. 423-433, Sep. 2011.

[31] S.I. Alekseev and M.C. Ziskin, "Influence of blood flow and millimeter wave exposure on skin temperature in different thermal model", *Biolectromagn.*, vol. 30, pp. 52-58, Jan. 2009.

[32] P.J. Riu, K.R. Foster, D.W. Blick, and E.R. Adair, "A thermal model for human thresholds of microwave-evoked warmth sensations", *Bioelectromagn.*, vol. 18, no. 8, pp. 578-583, Dec. 1997.

[33] M. Zhadobov, N. Chahat, R. Sauleau, C. Le Quément, and Y. Le Dréan, "Millimeter-wave interactions with the human body: State of knowledge and recent advances", *Int. J. Microw. Wirel. Tech.*, vol. 3, no. 2, pp. 237–247, Apr. 2011.

[34] G. Shafirstein and E.G. Moros, "Modelling millimeter wave propagation and absorption in a high resolution skin model: the effect of sweat glands", *Phys. Med. Biol.*, vol. 56, no. 5, pp. 1329-1339, Mar. 2011.

[35] S.I. Alekseev and M.C. Ziskin, "Local heating of human skin by millimeter waves: a kinetics study", *Bioelectromagn.*, vol. 24, no. 8, pp. 571-581, Dec. 2003.

[36] T.J. Walters, D.W. Blick, L.R. Johnson, E.R. Adair, and K.R. Foster, "Heating and pain sensation produced in human skin by millimeter waves: comparison to a simple thermal model", *Health Phys.*, vol. 78, no. 3, pp. 259-267, Mar. 2000.

[37] W.J. Ellison, "Permittivity of pure water, at standard atmospheric pressure, over the frequency range 0–25THz and the temperature range 0–100°C", *J. Phys. Chem.*, vol. 36, pp. 1-18, 2007.

[38] S. Gabriel, R.W. Lau, and C. Gabriel, "The dielectric properties of biological tissues: II. Measurements in the frequency range 10 Hz to 20 GHz", *Phys. Med. Biol.*, vol. 41, pp. 2251-2269, 1996.

[39] O.P. Gandhi and A. Riazi, "Absorption of millimeter waves by human beings and its biological implications", *IEEE Trans. Microw. Theory Tech.*, vol. 34, no. 2, pp. 228-235, Feb. 1986.

[40] C.M. Alabaster, "Permittivity of human skin in millimeter wave band", *Electron. Lett.*, vol. 39, no. 21, pp. 1521-1522, Oct. 2003.

[41] H. Hwang, J. Yim, J.W. Cho, C. Cheon, and Y. Kwon, "110 GHz broadband measurement of permittivity on human epidermis using 1 mm coaxial probe", *IEEE Int. Micro. Symp. Digest*, vol. 1, pp. 399-402, Jun. 2003.

[42] S.I. Alekseev and M.C. Ziskin, "Human skin permittivity determined by millimeter wave reflection measurements", *Bioelectromagn.*, vol. 28, no. 5, pp. 331-339, Jul. 2007.

[43] N. Chahat, M.Zhadobov, R. Sauleau, and S.I. Alekseev, "New method for determining dielectric properties of skin and phantoms at millimeter waves based on heating kinetics", *IEEE Trans. Microw. Theory Tech.*, vol. 60, no. 3, pp. 827-832, Mar. 2012.

[44] "MCL-T broadband tissue equivalent liquid: 30 MHz to 6 GHz," MCL-T, London, UK [Online]. Available: http://www.mcluk.org/pdfs/bbl.pdf

[45] A.W. Guy, "Analyses of electromagnetic fields induced in biological tissues by thermographic studies on equivalent phantom models", *IEEE Microw. Theory Techn.*, vol. 19, no. 2, pp. 205-214, Feb. 1971.

[46] "IEEE Recommended practice for determining the peak special-average specific absorption rate (SAR) in the human head from wireless communication devices: measurement techniques", *IEEE Standard 1528-2003*, 2003.

[47] K. Ito, K. Furuya, Y. Okano, and L. Hamada, "Development and characteristics of a biological tissue-equivalent phantom for microwaves", *Electron. Commun. Japan*, vol. 48, no. 4, pp. 67-77, Apr. 2001.

[48] Y. Okano, K. Ito, I. Ida, and M. Takahashi, "The SAR evaluation method by a combination of thermographic experiments and biological tissue-equivalent phantoms", *IEEE Microw. Theory Techn.*, vol. 48, no. 11, pp. 2094-2103, Nov. 2000.

[49] Y. Nikawa, M. Chino, and K. Kikuchi, "Soft and dry phantom modeling material using silicone rubber with carbon fiber", *IEEE Microw. Theory Techn.*, vol. 44, no. 10, pp. 1949-1953, Oct. 1996.

[50] H. Tamura, Y. Ishikawa, T. Kobayashi, and T. Nojima, "A dry phantom material composed of ceramic and graphite powder", *IEEE Trans. Electromagn. Compat.,* vol. 39, no. 2, pp. 132-137, May 1997.

[51] J.T. Chang, M.W. Fanning, P.M. Meaney, and K.D. Paulsen, "A conductive plastic for simulating biological tissues at microwave frequencies", *IEEE Trans. Electromagn. Compat.*, vol. 42, no. 1, pp. 76-81, Feb. 2000.

[52] T. Takimoto, T. Onishi, K. Saito, M. Takahashi, S. Uebayashi, and K. Ito, "Characteristics of biological tissue equivalent phantoms applied to UWB communications", *Electron. Commun. Japan*, vol. 90, no. 5, pp. 48-55, May 2007.

[53] J. Yonebayashi, S. Takamatsu, K. Saito, M. Takahashi, and K. Ito, "Development of dynamic phantom for evaluation of breath detection Doppler radar", *32nd Ann. Bioelectromagn. Soc. Meet.*, Seoul, Korea, pp. 297-299, Jun. 2010.

[54] C. Gabriel, "Tissue equivalent material for hand phantoms", *Phys. Med. Biol.*, vol. 53, no. 14, pp. 4205-4210, Jul. 2007.

[55] N. Chahat, M. Zhadobov, and R. Sauleau, "Broadband tissue-equivalent phantom for BAN applications at millimeter waves", *IEEE Microw. Theory Techn.*, vol. 60, no. 7, pp. 2259–2266, Jul. 2012.

[56] N. Chahat, G. Valerio, M. Zhadobov, and R. Sauleau, "On-body propagation at 60 GHz", *IEEE Trans. Antennas Propag.*, vol. 61, no. 4, pp. 1876–1888, Apr. 2013.

[57] A.R. Guraliuc, M. Zhadobov, G. Valerio, N. Chahat, and R. Sauleau, "Effect of textile on the propagation along the body at 60 GHz", *IEEE Trans. Antennas Propag.*, vol. 62, no. 3, pp. 1489-1494, Mar. 2014.

[58] A.R. Guraliuc, M. Zhadobov, O. De Sagazan, and R. Sauleau, "Solid phantom for body-centric propagation measurements at 60 GHz", *IEEE Microw. Theory Tech.*, vol. 62, no. 6, pp. 1373-1380, Jun. 2014.

[59] S.I. Alekseev, A.A. Radzievsky, M.K. Logani, and M.C. Ziskin, "Millimeter wave dosimetry of human skin", *Bioelectromagn.*, vol. 29, no. 1, pp. 65-70, Jan. 2008.

[60] K.R. Foster, H.N. Kritikos, and H.P. Schwan, "Effect of surface cooling and blood flow on the microwave heating of tissue", *IEEE Trans. Biomed. Eng.*, vol. 25, no. 8, pp. 313 – 316, May 1978.

[61] K. Ali, A. Brizzi, A. Pellegrini, Y. Hao, and A. Alomainy, "Investigation of the effect of fabric in on-body communication using finite difference time domain technique at 60 GHz", *Antennas Propag. Conf. (LAPC)*, Loughborough, U.K., Nov. 2012.

[62] C. Hertleer, A. Tronquo, H. Rogier, L. Vallozzi, and L. Van Langenhove, "Aperture-coupled patch antenna for integration into wearable textile systems", *IEEE Antennas Wirel. Propag. Lett.*, vol. 6, pp. 392–395, 2007.

[63] P. S. Hall, Y. Hao, Y. I. Nechayev, A. Alomainy, C. C. Constantinou, C. Parini, M. R. Kamarudin, T. Z. Salim, D. T.M. Hee, R. Dubrovka, A. S. Owadall, W. Song, A. A. Serra, P. Nepa, M. Gallo, and M.Bozzetti, "Antennas and propagation for on-body communication systems", *IEEE Antennas Propag. Mag.*, vol. 49, no. 3, pp. 41–58, Jun. 2007.

[64] P. S. Hall and Y. Hao, Antennas and Propagation for Body Centric Communications Systems. Norwood, MA, *USA: Artech House*, 2006.

[65] E. Reusens, W. Joseph, B. Latre, B. Braem, G. Vermeeren, E. Tanghe,L. Martens, I. Moerman, and C. Blondia, "Characterization of on-body communication channel and energy efficient topology design for wireless body area networks", *IEEE Trans. Inform. Technol. Biomed.*, vol. 13, no. 6, pp. 933–945, Nov. 2009.

[66] Y. I. Nechayev, Z. H. Hu, and P. S. Hall, "Short-term and long-term fading of on-body transmission channels at 2.45 GHz", *Antennas Propag. Conf. (LAPC)*, Loughborough, UK, Nov. 2009.

[67] A. R. Guraliuc, A. A. Serra, P. Nepa, and G. Manara, "Path gain models for on-body communication systems at 2.4 and 5.8 GHz", *Ann. Telecomm.*, vol. 66, no. 3–4, pp. 205–212, Apr. 2011.

[68] Q. H. Abbasi, A. Sani, A. Alomainy, and Y. Hao, "Numerical characterization and modeling of subject-specific ultra-wide band body-centric radio channels and systems for healthcare applications", *IEEE Trans. Inform. Technol. Biomed.*, vol. 16, no. 2, pp. 221–227, Mar. 2012.

[69] N. Chahat, M. Zhadobov, R. Sauleau, and K. Ito, "A compact UWB antenna for on-body applications", *IEEE Trans. Antennas Propag.*, vol. 59, no. 4, pp. 1123–1131, Apr. 2011.

[70] Y. I. Nechayev, X.Wu, C. C. Constantinou, and P. S. Hall, "Millimeter wave path loss variability between two body-mounted monopole antennas", *IET Microw. Antennas Propag.*, vol. 7, no. 1, pp. 1–7, Jan. 2013.

[71] A. Pellegrini, A. Brizzi, L. Zhang, K. Ali, Y. Hao, X. Wu, C.C. Constantinou, Y. Nechayev, P.S. Hall, N. Chahat, M. Zhadobov, and R. Sauleau, "Antennas and propagation for body centric wireless communications at millimeter wave frequencies: a review", *IEEE Antennas Propag. Mag.*, vol. 55, no. 4, pp. 262-287, Aug. 2013.

[72] S. Alipour, F. Parvaresh, H. Ghajari, and D. F. Kimbal, "Propagation characteristics for a 60 GHz wireless body area network (WBAN)", in *Proc. Military Commun. Conf.*, San Diego, CA, USA, pp. 719–723, Nov. 2010.

[73] T. Mavridis, L. Petrillo, J. Sarrazin, D. Lautru, A. Benlarbi-Delai, and P. De Doncker, "Theoretical and experimental investigation of a 60GHz off-body propagation model", *IEEE Trans. Antennas Propag.*, vol. 62, no. 1, pp. 393–402, Jan. 2014.

[74] T. Mavridis, L. Petrillo, J. Sarrazin, D. Lautru, A. Benlarbi-Delai, and P. De Doncker, "Creeping wave model of diffraction of an obliquely incident plane wave by a circular cylinder at 60 GHz", *IEEE Trans. Antennas Propag.*, vol. 62, no. 3, pp. 1372–1377, Mar. 2014.

[75] S. Collonge, G. Zaharia, and G. El Zein, "Influence of the human activity on wide-band characteristics of the 60 GHz indoor radio channel", *IEEE Trans. Wireless Comm.*, vol. 3, no. 6, pp. 2396-2406, Nov. 2004.

[76] C.H. Durney, H. Massoudi, and M.F. Iskander, "Radiofrequency Radiation Dosimetry Handbook", *USAF School of Aerospace Medicine*, Brooks AFB, TX, Report USAFSAM-TR-85-73, 1986.

[77] O.P. Gandhi, "Advances in dosimetry of radio-frequency radiation and their past and projected impact on the safety standards", *Proc. IMTC Instr. Meas. Tech. Conf.*, pp. 109-113, San Diego, CA, Apr. 20-22, 1988.

[78] P.W. Barber, "Electromagnetic power deposition in prolate spheroid models of man and animals at resonance", *IEEE Trans. Biomed. Eng.*, vol. 24, no. 6, pp. 513-521, Nov. 1977.

[79] C.H. Durney, C.C. Johnson, P.W. Barber, H. Massoudi, M.F. Iskander, J.L. Lords, D.K. Ryser, S.J. Allen, and J.C. Mitchell, "Radiofrequency radiation dosimetry handbook", *2nd Edition,* (Report SAM-TR-78-22)*, Brooks Air Force Base, USAF School on Aerospace Medicine*, TX 78235, 1978.

[80] "Vaughan & Asbury's General Ophthalmology - 18th ed.", edited by P. Riordan-Eva, and E.T. Cunningham, *New York: McGraw-Hill Medical*, ISBN 978-0071634205.

[81] K.S. Yee, "Numerical solution of initial boundary value problems involving Maxwell's equations in isotropic media", *IEEE Trans Ant. Propag.*, vol. 14, no. 3, pp. 302-307, May 1966.

[82] T. Weiland, "A discretization method for the solution of Maxwell's equations for six-component fields", *Electronics and Comm. AEUE*, vol. 31, no. 3, pp. 116-120, 1977.

[83] M. Ghaddar, L. Talbi, T. Denidni, and A. Sebak, "A Conducting Cylinder for Modeling Human Body Presence in Indoor Propagation Channel", *IEEE Trans. Ant. Propag.*, vol. 55, no. 11, pp. 3099-3103, Nov. 2007.

[84] S. L. Cotton, W. G. Scanlon, and B. K. Madahar, "Millimeter-wave soldier-to-soldier communications for covert battlefield operations", *IEEE Comm. Mag.*, vol. 47, no. 10, pp. 72-81, Oct. 2009.

[85] www.cst.com

[86] A. Christ, W. Kaintz, E.G. Hahn, K. Honegger, M. Zefferer, E. Neufeld, W. Rascher, R. Janka, W. Bautz, J. Chen, B. Kiefer, P. Schmitt, H.P. Hollenbach, J. Shen, M. Oberle, D. Szczrba, A. Kam, J.W. Guag, and N. Kuster, "The virtual family-development of surface-based anatomical models of two adults and two children for dosimetric simulations", *Phys. Med. Biol.*, vol. 55, no. 23, pp. N23-N36, 2010.